ISSN: 2162-6162 Volume 7, Number 3, September 2017

Scientific Research Publishing

# Journal of Electronics Cooling and Thermal Control

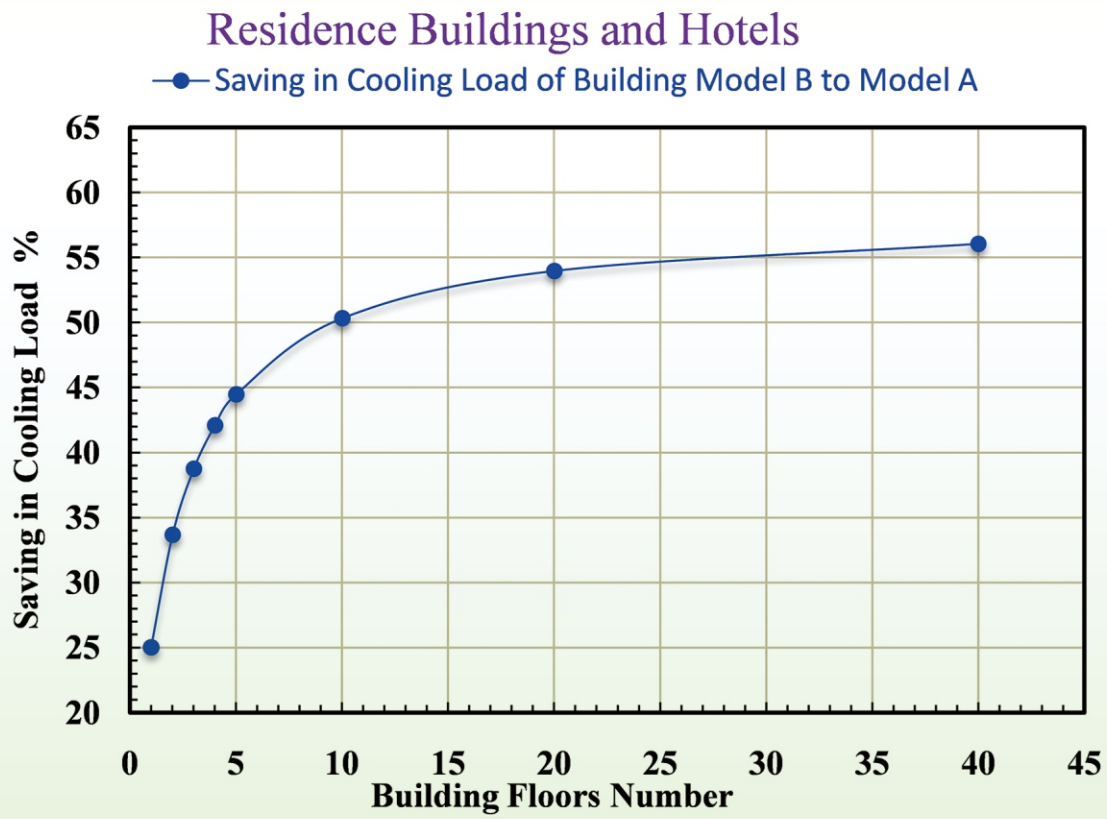


ISSN: 2162-6162

www.scirp.org/journal/jectc

# Journal Editorial Board

**ISSN 2162-6162 (print) ISSN 2162-6170 (online)**

**http://www.scirp.org/journal/jectc**

## Editor-in-Chief

Scientific Research Publishing

Journal of Electronics Cooling and Thermal Control, 2017, 7, 45-89
http://www.scirp.org/journal/jectc
ISSN Online: 2162-6170
ISSN Print: 2162-6162

# Table of Contents

Volume 7 Number 3 September 2017



The figure on the front cover is from the article published in Journal of Electronics Cooling and Thermal Control, 2017, Vol. 7, No. 3, pp. 45-62 by Mousa M. Mohamed and Mohammed Hueesin Almarshadi.

# Journal of Electronics Cooling and Thermal Control (JECTC)
# Journal Information

## SUBSCRIPTIONS

The *Journal of Electronics Cooling and Thermal Control* (Online at Scientific Research Publishing, www.SciRP.org) is published quarterly by Scientific Research Publishing, Inc., USA.

**Subscription rates:**
Print: $79 per issue.
To subscribe, please contact Journals Subscriptions Department, E-mail: sub@scirp.org

## SERVICES

**Advertisements**
Advertisement Sales Department, E-mail: service@scirp.org

**Reprints (minimum quantity 100 copies)**
Reprints Co-ordinator, Scientific Research Publishing, Inc., USA.
E-mail: sub@scirp.org

## COPYRIGHT



## PRODUCTION INFORMATION

For manuscripts that have been accepted for publication, please contact:
E-mail: jectc@scirp.org

Journal of Electronics Cooling and Thermal Control, 2017, 7, 45-62
http://www.scirp.org/journal/jectc
ISSN Online: 2162-6170
ISSN Print: 2162-6162

# Simulation of District Cooling Plant and Efficient Energy Air Cooled Condensers (Part I)

**Mousa M. Mohamed[1], Mohammed Hueesin Almarshadi[2]**

[1]Mechanical Power Engineering, Faculty of Engineering, Menoufia University Shebin El kom, Egypt
[2]Arid Land Agriculture Department, Faculty of Meteorology, Environment and Arid Land Agriculture, King Abdulaziz University, Jeddah, KSA
Email: mousamohamed@yahoo.com, malmarshadi@kau.edu.sa

**How to cite this paper:** Mohamed, M.M. and Almarshadi, M.H. (2017) Simulation of District Cooling Plant and Efficient Energy Air Cooled Condensers (Part I). *Journal of Electronics Cooling and Thermal Control*, **7**, 45-62.
https://doi.org/10.4236/jectc.2017.73005

**Received:** May 18, 2017
**Accepted:** July 18, 2017
**Published:** July 21, 2017



## Abstract

In hot arid countries with severe weather, the summer air conditioning systems consume much electrical power at peak period. Shifting the loads peak to off-peak period with thermal storage is recommended. Model A of residential buildings and Model B of schools and hospitals were used to estimate the daily cooling load profile in Makkah, Saudi Arabia at latitude of 21.42˚N and longitude of 39.83˚E. Model A was constructed from common materials, but Model B as Model A with 5 - 8 cm thermal insulation and double layers glass windows. The average data of Makkah weather through 2010, 2011 and 2012 were used to calculate the cooling load profile and performance of air conditioning systems. The maximum cooling load was calculated at 15:00 o'clock for a main floor building to a 40-floor of residential building and to 5 floors of schools. A district cooling plant of 180,000 Refrigeration Ton was suggested to serve the Gabal Al Sharashf area in the central zone of Makkah. A thermal storage system to store the excess cooling capacity was used. Air cooled condensers were used in the analysis of chiller refrigeration cycle. The operating cost was mainly a function of electrical energy consumption. Fixed electricity tariff was 0.04 $/kWh for electromechanical counter, and 0.027, 0.04, 0.069 $/kWh for shifting loads peak for the smart digital counter. The results showed that the daily savings in consumed power are 8.27% in spring, 6.86% in summer, 8.81% in autumn, and 14.55% in winter. Also, the daily savings in electricity bills are 12.26% in spring, 16.66% in summer, 12.84% in autumn, and 14.55% in winter. The obtained maximum saving in consumed power is 14.5% and the daily saving in electricity bills is 43% in summer when the loads peak is completely shifted to off-peak period.

## Keywords

District Cooling, Thermal Storage System, Cooling Load Profile, Refrigeration

Capacity, Shifting Loadspeak, Saving in Electricity Bills, Saving Power, Efficient Energy

## 1. Introduction

In recent years, hot weather countries and areas like Qatar, UAE, Saudi Arabia, Singapore, Malaysia and Hong-Kong have installed a large scale district cooling plant. At the same time, other hot weather countries are the potential followers of such networks, while installation of centralized chiller plants for individual buildings is already a trend [1]. District cooling system uses thermal energy in the form of chilled water from a central plant to multiple buildings through a distribution network of underground insulated pipes for use in space cooling. The cooling process takes place in the central plant which eliminates the use of separate conventional cooling system from each building. The district cooling plant primarily consists of three components namely, the central cooling system, the distribution network and the energy transfer buildings [2]. The cooling equipment, cooling towers, power generation and thermal storage system are the main components of a central cooling system. The distribution system is insulated pips network that transfers the cooling medium or chilled water from the central cooling system to different energy transfer buildings. The energy transfer buildings contain indoor heat exchanger, secondary pumping system, chilled water piping and other auxiliary equipments.

A large-scale of district cooling plant could save energy consumption costs from 25% to 40% as compared with the sum of conventional centralized air-conditioning system of each building. In addition to a better energy efficiency, there are other environmental and planning benefits such as, reduced water consumption, reduced carbon footprint, minimized noise and vibration impact, flexibility in building design, saving in plant room space, reduced operating redundancy and enhanced system reliability [3] [4]. District cooling plant supplies cooling services at the temperature level of 5˚C - 7˚C, while with an expected return temperature of 12˚C - 15˚C. The central cooling plant is mostly assisted with a cold thermal storage unit, which allows the leveling of the cooling loads in the network during the day or season and creates a match in supply and demand of cooling services [5] [6]. Thus, a district cooling network with 8˚C and 15˚C as the supply-return temperature should be an ideal one. Positive to this configuration is lower energy loss and higher system efficiency. The energy use in a large district cooling plant before and after the addition of stratified chilled-water storage has been conducted and the average efficiency of the system improved by more than 10% [7].

The chilled water storage system has been constructed and is fully operational. The system is the largest stratified chilled water storage and the first to transfer the full air conditioning load to off-peak in Australia. The system gives approx-

imately 45% total spare capacity in its current system [8]. The optimal energy dispatch of an ice storage air-conditioning system has been simulated on a real air-conditioning system [9]. The data including the return temperature of chilled water, the supply temperature of chilled water, the return temperature of ice storage, and the supply temperature of ice storage are measured. The least-squares regression is used to obtain the input-output curve for the cooling load and power consumption of chillers and ice storage tank. The electricity savings on a summer day and on a non-summer day are 2.89% and 8.25%, respectively.

Therefore, the application of thermal energy storage has gained attractively to reduce energy cost. Many attractive tariff packages are being offered by the electricity provider to promote thermal energy storage. The tariff packages offered higher cost of electricity during peak period and lower cost of electricity during off-peak period. The results showed the energy required for running air condition unit and with of thermal energy storage. There are 36.5% - 37.82% total energy powers saving during peak period and this power saving manages to reduce maximum demand charge. Also, from the economic analysis conducted, it is found that the initial investment will recover in 5.41 years and is considered as a good investment whereby the initial cost is recovered less than 7 years [10].

The objective of the present study is to investigate the effect of hourly and seasonal environmental conditions, the building cooling load profile on the performance of refrigeration cycle and consumed power. The shifting of consumed power of the refrigeration capacity demand at peak to off-peak period with thermal storage system is proposed. The electric cost savings of consumed power with tariff packages are being offered by the electricity provider to promote the thermal storage system. Air cooled condensers for chillers refrigeration cycle are used to examine the daily power consumption and the reduction cost of electricity bills.

## 2. Building Models

The building cooling load is calculated according to the building specification and construction materials. **Figure 1** shows the layout of two types of buildings, the first is residential buildings and hotels; the second is schools and governmental buildings. Two Models A and B were used for the two types of buildings.

The buildings Model A is constructed from common materials; hollow bricks, heavy concrete, single layer glazed windows, and wooden doors as illustrated in **Figure 2**, but the buildings Model Bistypical as Model A of construction materials in addition of 5 - 8 cm thermal insulation of 0.039 W/m·K in outside walls, floor, ceiling and glazed windows with double layers of air gab 1 - 3 cm. The peak or maximum building heat load is estimated at 3 o'clock PM for outside condition of 45˚C dry bulb and 28˚C wet bulb and inside condition of 24˚C dry bulb and 50% relative humidity.

The building heat load is the amount of heat removed or added to the conditioned space to maintain the thermal comfort. The building heat load is divided

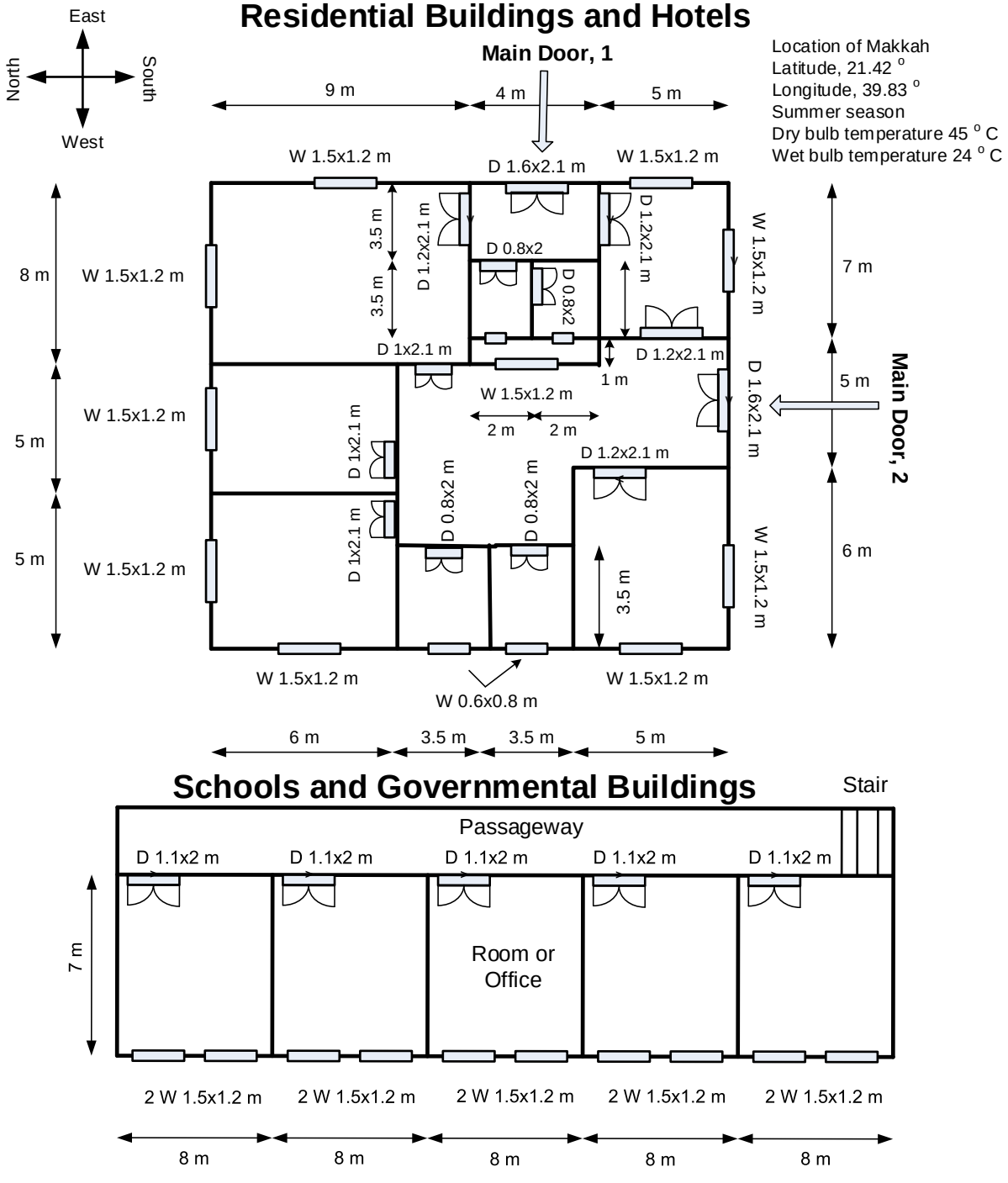


Figure 1. Layout residence buildings and schools.

in two heat loads, the first heat load is the sensible heat load which is a function of temperature difference between outside and inside condition, and radiation heat through glazing windows. The second heat load is the latent heat load which is a function of humidity ratio difference between outside and inside condition, and moisture content of conditioned space. The building heat load in

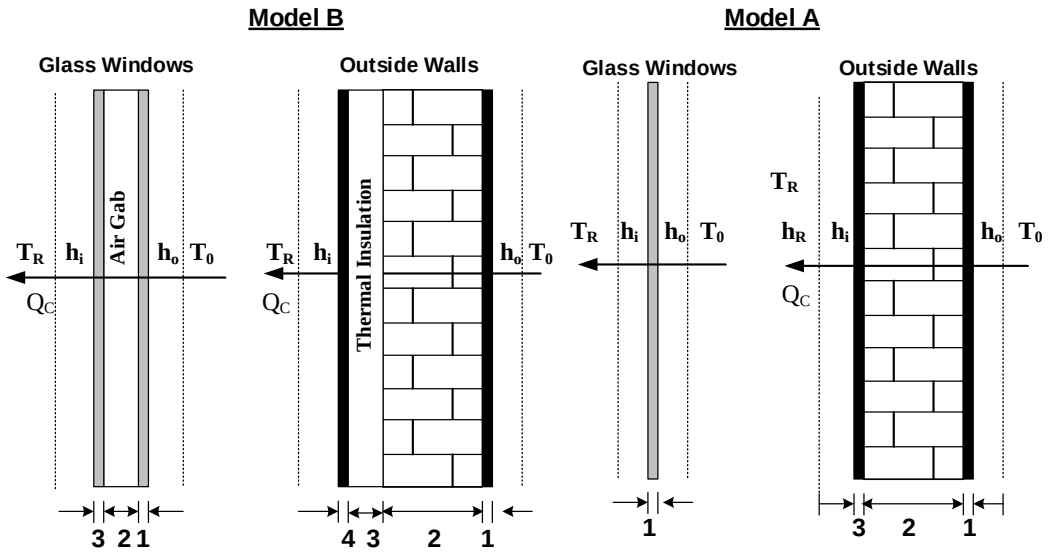


**Figure 2.** Building Models A and B with common construction materials and thermal insulation.

summer is the summation of external and internal heat loads. But, the building heat load in winter is the difference between the external and internal heat loads. The building cooling load in summer is calculated using appropriate cooling load temperature difference, CLTD method [11]. A computer program is prepared and examined. The data needed according to CLTD method for outside environment and building specification are inserted as subroutine to get the final results of hourly building cooling load.

The building cooling load of two Models A and B, are estimated as a floor area to Ton of Refrigeration from 1 to 40 floors for residence buildings and hotels, and from 1 to 5 floors for schools and government buildings. For buildings Model A and B, **Figures 3-6** show the required floor area of conditioned space to Ton of Refrigeration and percentage of saving in cooling load. It is observed that for main floor, 1 Ton of Refrigeration is enough to 16 $m^2$ of floor area for residence buildings and hotels of Model A and 21 $m^2$ of Model B, and these values increased gradually with floors number until 25 floors as shown in **Figure 3**. The saving in cooling load of Model A to Model B for residence buildings and hotels is 25% for main floor and 55% for 25 floors as illustrated in **Figure 4**. For schools and government buildings, the 1 Ton of Refrigeration is enough to 7.5 $m^2$ of floor area for main floor of Model A and 10 $m^2$ for main floor of Model B, and significant increase until 5 floors is observed as shown in **Figure 5**. The saving in cooling load of Model A to Model B for schools and government buildings is 34% for main floor and 45% for 5 floors as illustrated in **Figure 6**. Substantial increase in floor area, $m^2$/TR until 10 floors for residence buildings and 4 floors for schools are observed.

## 3. Building Cooling Load Profile

Makkah weather data for years, 2010, 2011, and 2012 at 21 day for each month

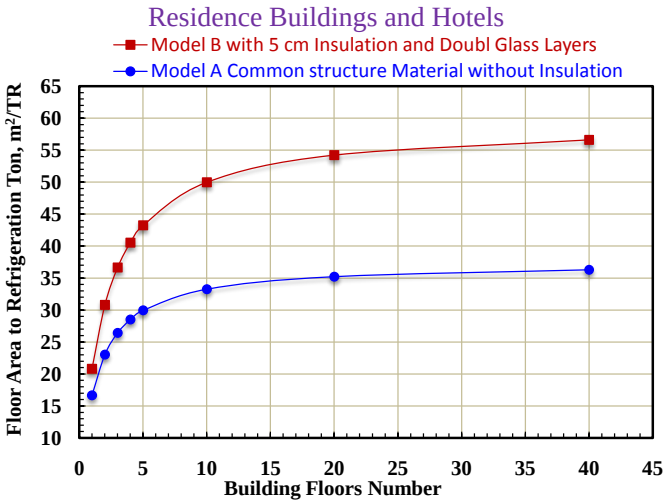


**Figure 3.** Floor area m²/TR for residence buildings and hotels.

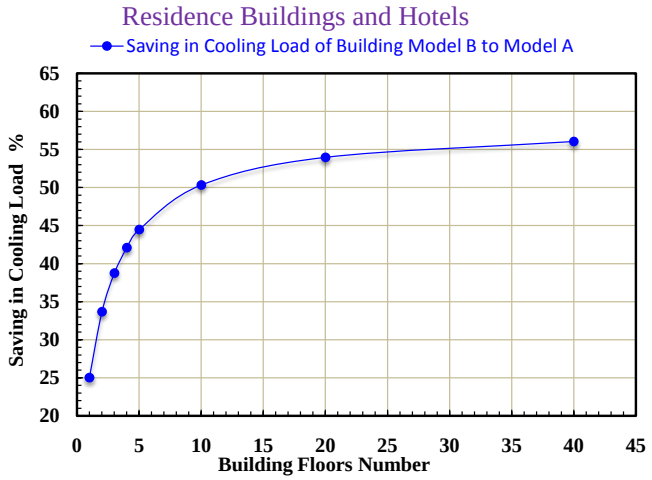


**Figure 4.** Percentage saving in cooling load for residence buildings and hotels.

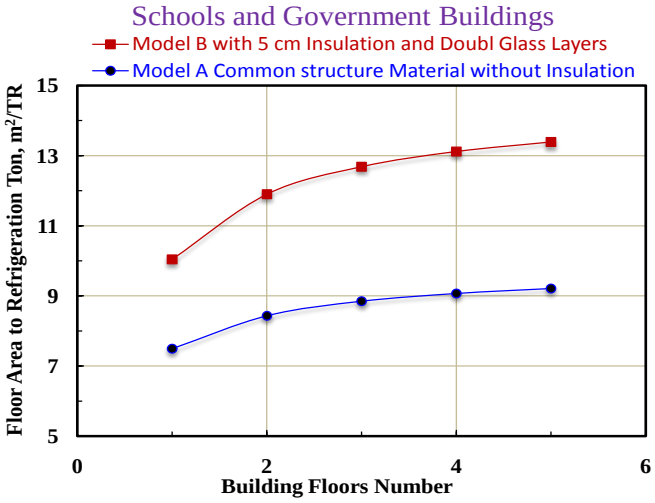


**Figure 5.** Floor area m²/TR for schools and government buildings.

are imported from meteorological station. The average data of dry bulb temperature, dew point temperature, and relative humidity for each season are estimated and illustrated in Figure 7 and Figure 8. The dry bulb temperature is increased hourly from sunrise to maximum value at 15:00 o'clock and decreased to initial value at night as shown in Figure 7. Opposite the trend of dry bulb temperature, the relative humidity decreased from sunrise to minimum value at 15:00 o'clock and increased to maximum value at night as shown in Figure 8. The building cooling load profile during four seasons, spring, summer, autumn, and winter are calculated and illustrated in Figure 9. The maximum building cooling load was happened at 16 o'clock. The cooling load profile in spring and

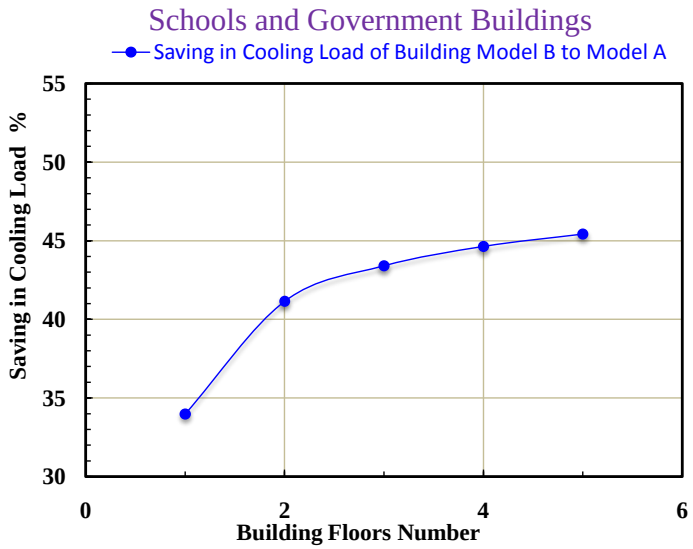


Figure 6. Save in cooling load for schools and government buildings.

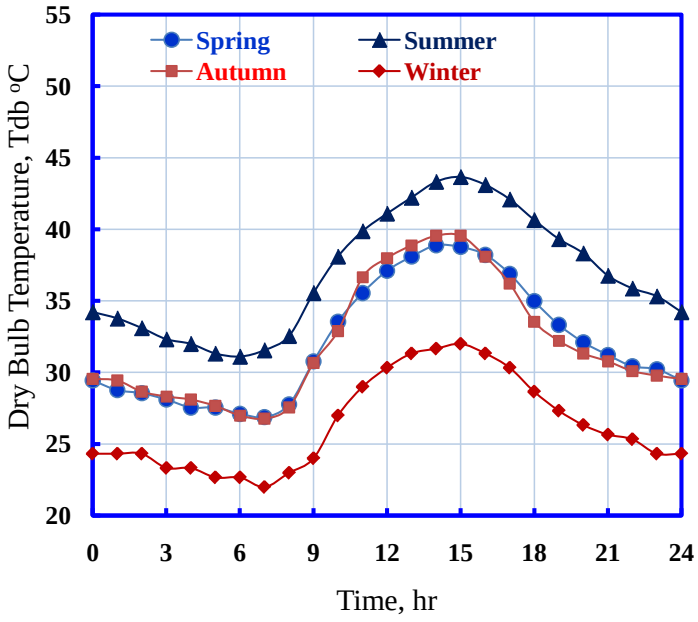


Figure 7. Average of dry bulb temperature.

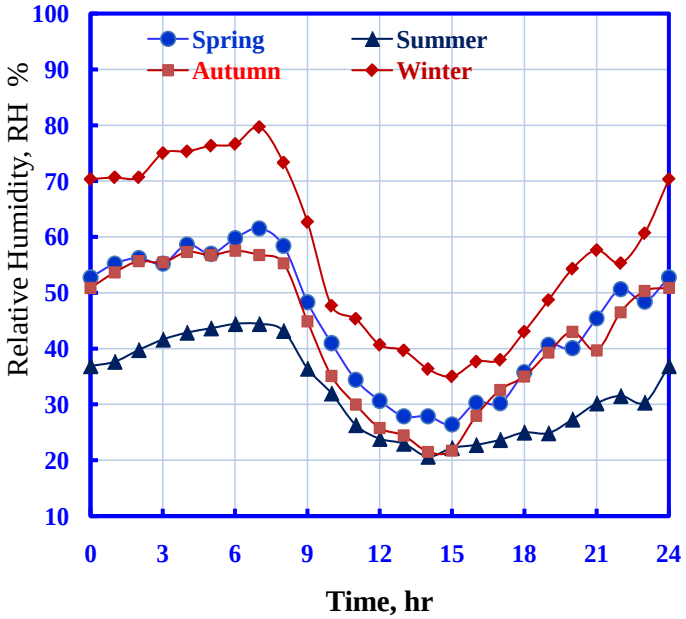


Figure 8. Average of relative humidity.

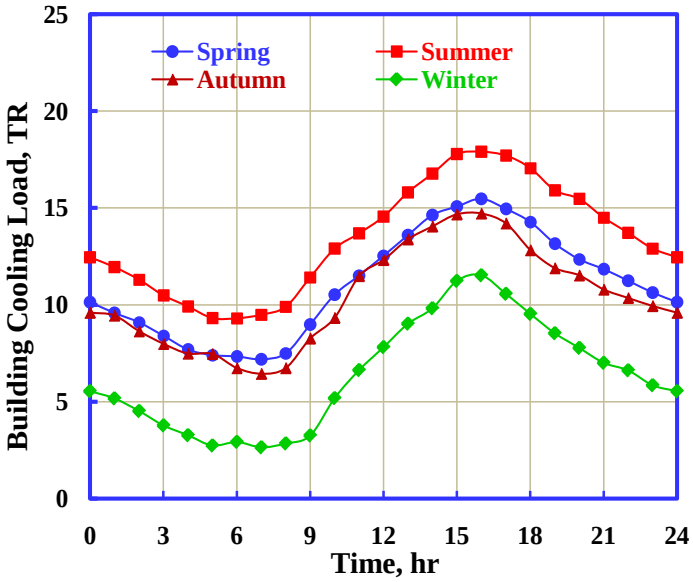


Figure 9. Building cooling load profile.

autumn is the same trend with small difference. The hourly building cooling load was divided on the maximum value at 16 o'clock to get the trend ratio of demand cooling load for simulation the hourly cooling load for district cooling plant as shown in Figure 10.

## 4. Refrigeration Capacity Analysis

A compression refrigeration machine with air cooled condenser is proposed. A simple refrigeration cycle is assumed with constant evaporating temperature of −1˚C and condensing temperature of 10 degrees above outside dry bulb temper

ature. The compression process with 80%isentropic efficiency is assumed and pressure drop of 0.5 bar in suction and delivery lines is appointed. The superheating temperature is 1˚C in suction line and sub-cooled temperature is 5˚C in liquid line. The CoolPack program [12] is used in the analysis of refrigeration cycle to estimate the Coefficient of Performance, COP, and compressor consumed power. The Makkah weather is hot and dry in summer through the daytime. The coefficient of performance, COP, of the refrigeration machine with air cooled condenser is very sensitive to the hourly change of outside air temperature. The COP is inversely proportional with the outside air temperature as shown in Figure 11. So, the COP of refrigeration cycle is much better during night than daytime. So, the operation of refrigeration machine after sunset to sunrise is much economical because the compressor consumes less power.

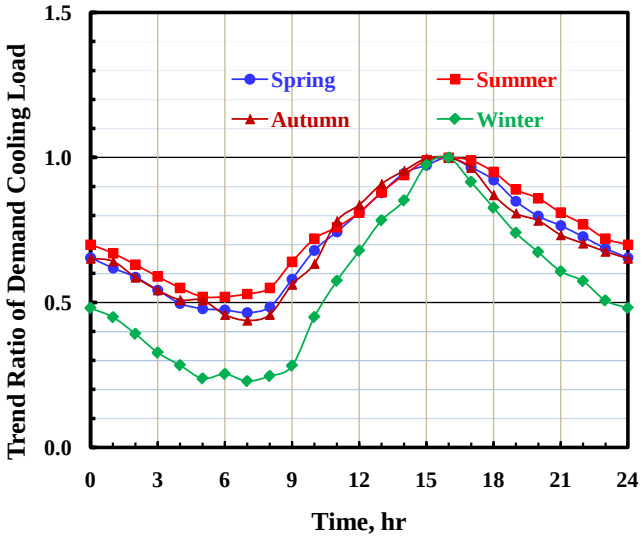


Figure 10. Trend ratio of demand cooling load to maximum.

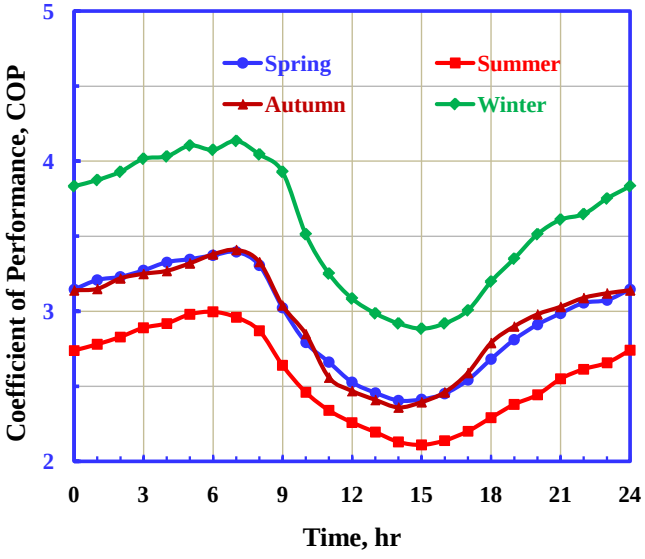


Figure 11. Hourly COP of refrigeration machine.

## 5. Electricity Tariffs

The thermal storage system is suggested to store the cooling capacity for later use at peak hours. There are two main operating strategies, the first is a full load operation and second is a partial load operation [13] [14]. Full load operation strategy, the cooling loads at peak period is supplied by the thermal storage while the chillers operate only at nighttime. In the partial load operation strategy, some chillers and thermal storage are used to supply the building cooling loads in peak periods simultaneously. In this study, the two main operating strategies are used. Firstly, the partial load operation strategy is used to transfer the peak loads to off-peak period. The demand cooling loads at peak are covered partially from thermal storage system and running some chillers. In off-peak period, all chillers running at full capacity and the excess cooling capacity are stored. Secondly, the full load operation strategy is used to transfer the loads peak to off-peak period which the demand cooling loads at peak period are covering from thermal storage only and all chillers off.

The electricity company in Saudi Arabia is supplying the electrical energy with two tariffs. The first tariff is fixed with electromechanical counter and the second tariff is variable with smart digital counter to courage consumers to shift the loads peak to off-peak period as Table 1.

## 6. Demand Cooling Load for Gabal Al Sharashf

The buildings construction conditions for Gabal Al Sharashfregion are illustrated in Table 2. The demand cooling loads of Gabal Al Sharashf inside the central zone of Makkah city is calculated with data in Table 2 according to the buildings model A and floors number. So, the obtained cooling capacity is 180,000 TR, and it is used as a maximum cooling load to find the demand cooling

Table 1. Electricity tariffs for contracted customers above 1000 KVA.

| Consumption period | Electromechanical counter | | Smart digital counter | |
|---|---|---|---|---|
| | Period | Tariff, $/kWh | Period | Tariff, $/kWh |
| 1st October-31 April | 24 hours | 0.0373 | 24 hours | 0.0373 |
| 1st May-31 September | 24 hours | 0.04 | Saturday → Thursday<br>00:00 AM → 08:00 AM<br>Friday (Weekend)*<br>00:00 AM → 09:00 AM<br>21:00 PM → 00:00 AM | 0.0267 |
| | | | Peak period<br>Saturday → Thursday<br>12:00 PM → 17:00 PM | 0.0693 |
| | | | Off-peak period | 0.04 |

United State Dollar, USD, $ and Saudi Arabia Riyal, SAR: Currency, 1 USD, $ = 3.75155 SAR. *Friday in Saudi Arabia is the week end holiday.

Table 2. Construction conditions for Gabal Al Sharashf region.

| Using | Land area | | Construction area | | Demand cooling load | | |
|---|---|---|---|---|---|---|---|
| | $m^2$ | % | $m^2$ | % | Floors No. | $m^2$/TR | TR |
| Residence | 236,782 | 14.5 | 1,099,122 | 23.8 | 5 | 29 | 37,901 |
| Commercial residence | 406,794 | 24.9 | 2,513,579 | 54.3 | 6 | 30 | 83,786 |
| Residence seasonal | 140,148 | 8.6 | 539,464 | 11.7 | 4 | 28 | 19,267 |
| Commercial | 78,105 | 4.8 | 416,867 | 9.0 | 5 | 29 | 14,375 |
| Educational service | 47,726 | 2.9 | 32,124 | 0.7 | 1 | 7.5 | 4283 |
| Healthy service | 18,977 | 1.2 | 12,410 | 0.3 | 1 | 7.5 | 1655 |
| Religion service | 19,470 | 1.2 | 12,649 | 0.3 | 1 | 7.5 | 1687 |
| Policy service | 952 | 0.1 | 952 | 0.02 | 1 | 7.5 | 127 |
| Green Area | 125,790 | 7.7 | | | | | |
| Streets | 559,201 | 34.2 | | | | | |
| Total | 1,633,946 | 100 | 4,627,167 | 100 | | | 163,079 |
| Assume safety factor of 10% | Total demand cooling load | | | | 180,000 TR | | |

loads profile through 24 hours. The hourly demand refrigeration capacity and compressor consumed power for maximum cooling load of 180,000 TR are estimated for conducting the scenarios of transferring the loads peak to off-peak period.

## 7. Shifting Loads Peak Scenarios

The scenarios of shifting loads peak to off-peak period are depend on the rated chillers capacity and thermal storage tank size. We assumed that the thermal storage tank size is enough to store the excess refrigeration capacity of chillers during off-peak period. The scenarios used to shifting loads peak period are how we decrease the load peak to minimum value to achieve the maximum saving in consumed power and minimum cost of electricity bills. The first scenario is conducted for rated chillers capacity of 180,000 TR which is equal the maximum demand cooling load at 16:00 o'clock. Figure 12 and Figure 13 show the scenario of shifting load peak from 12:00 to 17:00 o'clock in summer which 25% only of rated chillers capacity is running and other chillers off. The consumed power is decreased by 6.86% and the saving of electricity bills are 16.66%. Figures 14-17 show the scenario of shifting loads peak from 11:00 to 18:00 o'clock in spring and autumn which 17% only of rated chillers capacity are running and other chillers off. The consumed power is decreased by 8.54% and the saving of electricity bills are 12.55%. Figure 18 and Figure 19 show the scenario of shifting loads peak from 11:00 to 20:00 o'clock in winter which 100% of rated chillers capacity off. Both the decreasing in consumed power and the saving of electricity bills are 14.55%.

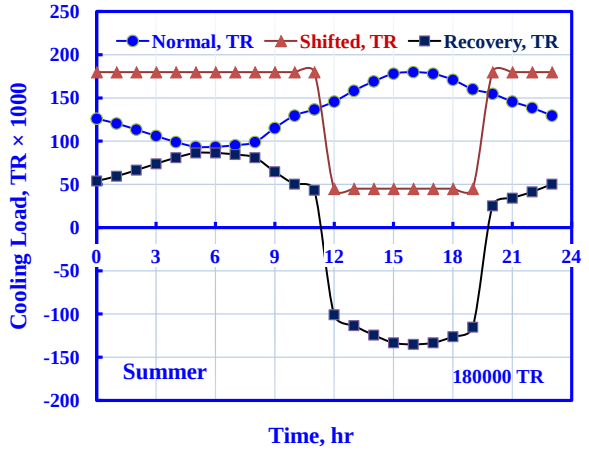


**Figure 12.** Summer scenario of cooling load for capacity of 180,000 TR.

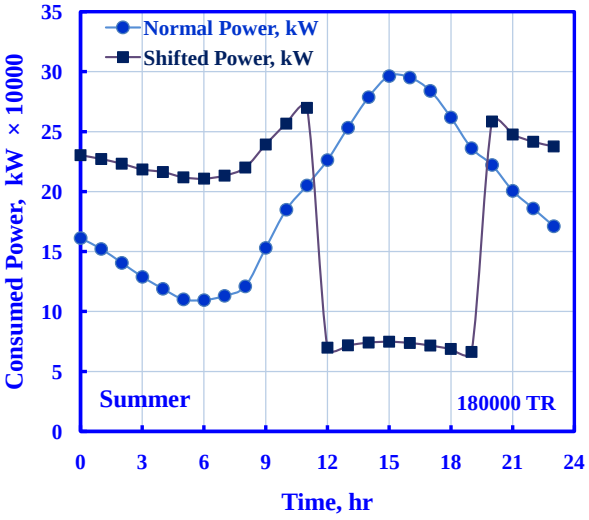


**Figure 13.** Summer scenario of consumed power for capacity of 180,000 TR.

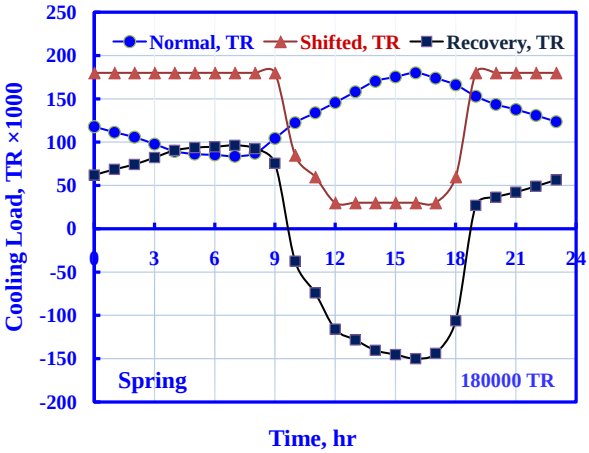


**Figure 14.** Spring scenario of cooling load for capacity of 180,000 TR.

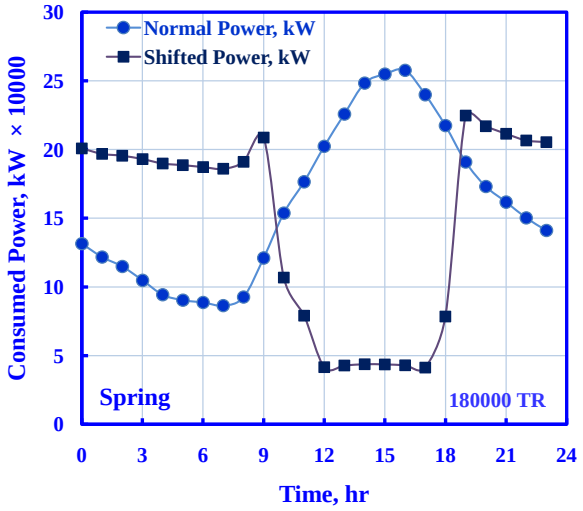


**Figure 15.** Spring scenario of consumed power for capacity of 180,000 TR.

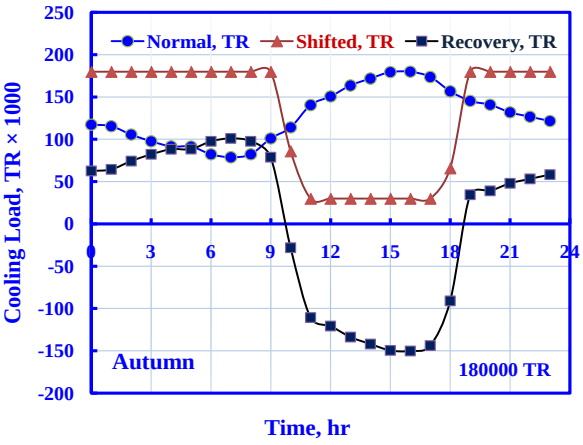


**Figure 16.** Autumn scenario of cooling load for capacity of 180,000 TR.

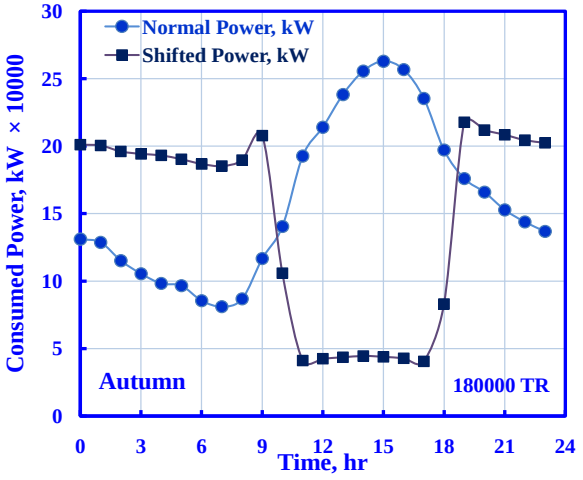


**Figure 17.** Autumn scenario of consumed power for capacity of 180,000 TR.

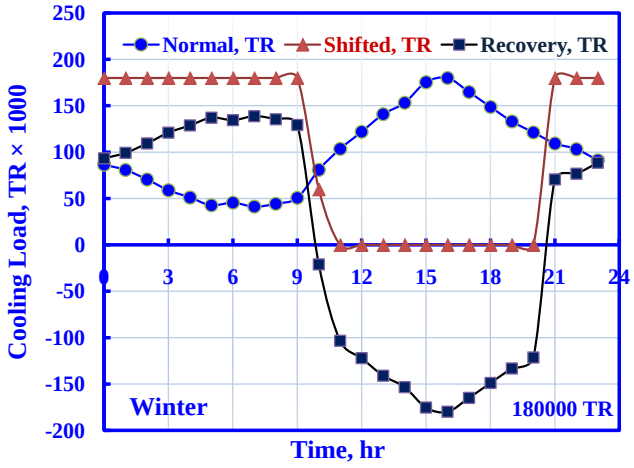


Figure 18. Winter scenario of cooling load for capacity of 180,000 TR.

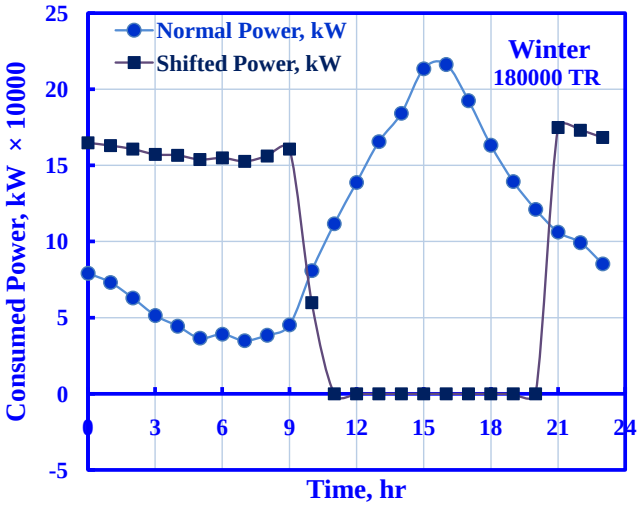


Figure 19. Winter scenario of consumed power for capacity of 180,000 TR.

The other scenarios are conducted by increasing the rated chillers capacity to transfer the peak loads to off-peak period, full load operation strategy. Because the discount of electricity cost is available from 1st of May to end of September. We will show some scenarios of summer with various rated chillers capacity as shown in Figures 20-23.

The rated chillers capacity is increased by 11% up to 122% with constant cooling load demand profile to investigate the maximum saving in consumed power and minimum cost of electricity bills as summarized in Table 3. The aim of increasing the rated chillers capacity in the plant is to transfer the loads peak to zero loads and extend the zero loads period gradually to minimize the consumed power and electricity bills as shown in Figure 24 and Figure 25. The increase in saving of consumed power in spring, summer and autumn is dominant than winter because the demand cooling load is low in winter. Also, the increase

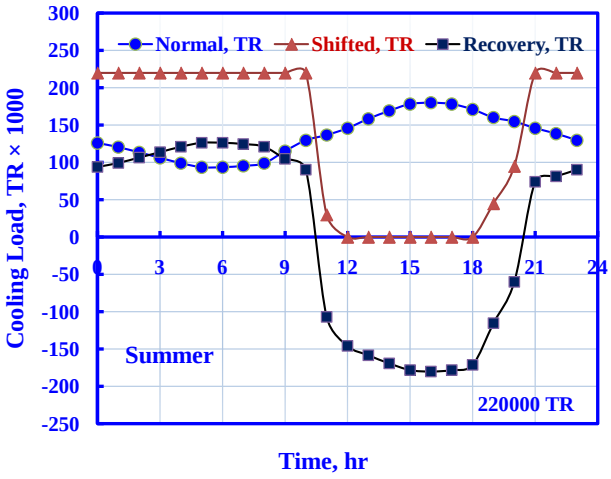


**Figure 20.** Summer scenario of cooling load capacity of 220,000 TR.

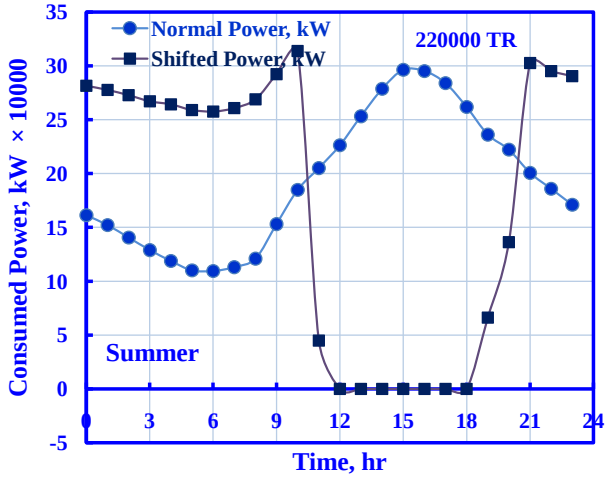


**Figure 21.** Summer scenario of consumed power for capacity of 220,000 TR.

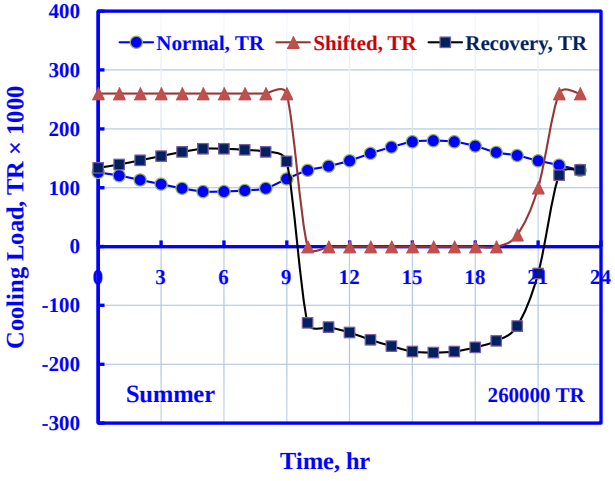


**Figure 22.** Summer scenario of cooling load for capacity of 260,000 TR.

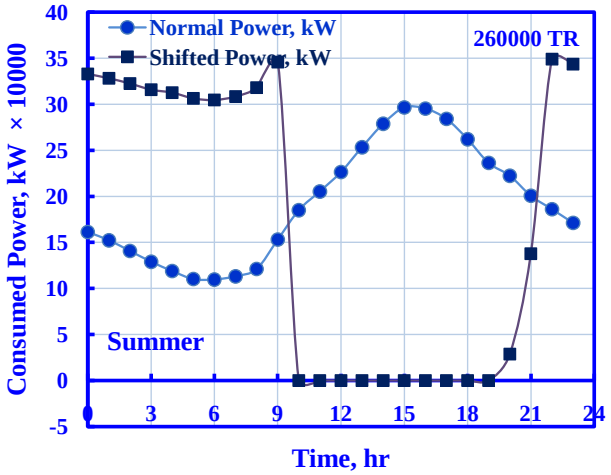


**Figure 23.** Summer scenario of consumed power for capacity of 260,000 TR.

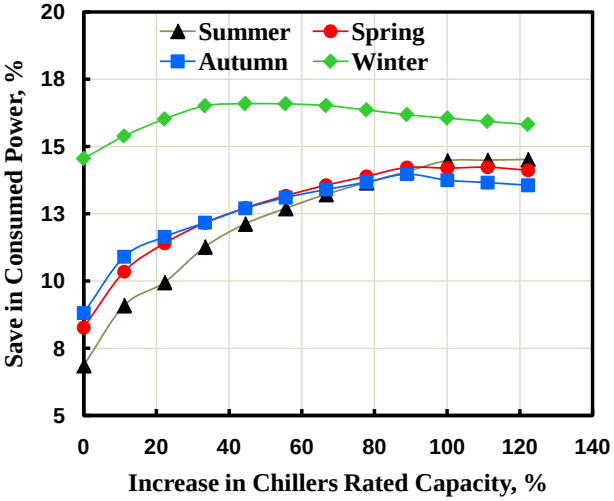


**Figure 24.** Save in consumed power.

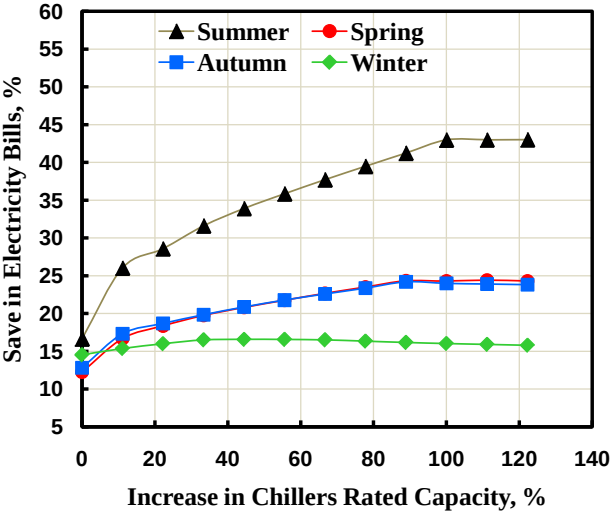


**Figure 25.** Save in electricity bills cost.

**Table 3.** Saving in consumed power and electricity bills cost.

| Chillers capacity needed | | Saving in consumed power, % | | | | Saving in electricity bills, % | | | |
|---|---|---|---|---|---|---|---|---|---|
| Chillers rated capacity, TR | Increase in chillers capacity % | Summer | Spring | Autumn | Winter | Summer | Spring | Autumn | Winter |
| 180,000 | 0 | 6.86 | 8.27 | 8.81 | 14.55 | 16.66 | 12.26 | 12.84 | 14.55 |
| 200,000 | 11 | 9.09 | 10.35 | 10.90 | 15.39 | 26.04 | 16.71 | 17.33 | 15.39 |
| 220,000 | 22 | 9.95 | 11.40 | 11.64 | 16.02 | 28.59 | 18.38 | 18.70 | 16.02 |
| 240,000 | 33 | 11.27 | 12.16 | 12.17 | 16.51 | 31.61 | 19.77 | 19.85 | 16.51 |
| 260,000 | 44 | 12.12 | 12.72 | 12.70 | 16.59 | 33.92 | 20.83 | 20.88 | 16.59 |
| 280,000 | 56 | 12.70 | 13.17 | 13.10 | 16.58 | 35.86 | 21.78 | 21.79 | 16.58 |
| 300,000 | 67 | 13.22 | 13.56 | 13.40 | 16.52 | 37.71 | 22.67 | 22.61 | 16.52 |
| 320,000 | 78 | 13.66 | 13.89 | 13.67 | 16.36 | 39.49 | 23.51 | 23.38 | 16.36 |
| 340,000 | 89 | 14.07 | 14.22 | 13.97 | 16.18 | 41.24 | 24.34 | 24.20 | 16.18 |
| 360,000 | 100 | 14.47 | 14.20 | 13.75 | 16.05 | 42.98 | 24.31 | 24.00 | 16.05 |
| 380,000 | 111 | 14.49 | 14.23 | 13.66 | 15.93 | 43.00 | 24.43 | 23.92 | 15.93 |
| 400,000 | 122 | 14.52 | 14.12 | 13.56 | 15.82 | 43.01 | 24.33 | 23.84 | 15.82 |

in saving of electricity bills in summer is dominant than spring, autumn and winter because the electricity tariff during off-peak period is cheap. The importance of data in Table 3 and Figure 24 and Figure 25 are for economic analysis and payback period for minimize the rated chillers capacity needed and thermal storage tank size. Payback Period is defined as the length of time required to recover an initial investment through cash flows generated by the investment. The Payback Period gives the level of profitability of an investment in relation to time. The shorter the period is the better the investment opportunity [10]. The payback period of initial investment of the system is not our interest in this paper.

## 8. Conclusion

A simulation of district cooling plant is performed. Shifting the load peak to off-peak period is recommended with thermal storage system. A model of residence buildings and schools is used to estimate the daily cooling load profile in Makkah, Saudi Arabia at latitude of 21.42˚ and longitude of 39.83˚. District cooling plant of 180,000 Ton of Refrigeration is suggested to serve the Gabal Al Sharashf area in central zone at Makkah. Fixed electricity tariff is 0.04 $/kWh for electromechanical counter, and 0.0267, 0.04, 0.0693 $/kWh for shifting loads peak for smart digital counter. The results showed that the savings in consumed power are 8.27% in spring, 6.86% in summer, 8.81% in autumn, and 14.55% in winter. But, the savings in electricity bills are 12.26% in spring, 16.66% in summer, 12.84% in autumn, and 14.55% in winter. The obtained maximum saving in consumed power is 14.5% and the saving in electricity bills is 43% in summer when transferring the loads peak to off-peak period.

## References


[1] Chow, T.T., *et al.* (2004) Applying District-Cooling Technology in Hong Kong. *Applied Energy*, **79**, 275-289.

[2] Augusto, G.L., *et al.* (2013) Identification of Design Criteria for District Cooling Distribution Network. *Philippine Science Letters*, **6**.

[3] Bin Shafar, A. (2011) Exclusive Interview of Empower CEO, Ahmad Bin Shafar by Michael Palmer. Dubai UAE.

[4] Lo, A., *et al.* (2014) Challenges of District Cooling System (DCS) Implementation in Hong Kong. World SB 14, Barcelona.

[5] Chow, T.-T., *et al.* (2006) Performance Evaluation of District Cooling Plant with Icestorage. *Energy*, **31**, 2750-2762.

[6] Hossain, M.K. (2004) Ice Slurry Storage System in District Cooling Applications for Air Conditioning. Master's Thesis, National University of Singapore, Singapore.

[7] Bahnfleth, W.P. and Joyce, W.S. Energy Use in District Cooling System with Stratified Chilled-Water Storage. ASHRAE Transactions: Symposia, No. 94-32-4.

[8] Beagley, S. (1999) A Chilled Water Storage System as Part of an Energy Management System. Facilities Management Division Northern Territory University, Darwin NT 0909, Australia. http://www.ntu.edu.au

[9] Lin, W.-M., *et al.* (2015) Optimal Energy Reduction Schedules for Ice Storage Air-Conditioning Systems. *Energies*, **8**, 10504-10521. https://doi.org/10.3390/en80910504

[10] Noranai, Z. and MdYusof, M.Z. (2011) Economical Analysis of Thermal Energy Storage by Partially Operation. *Int. J. Mechanical, Aerospace, Industrial, Mechatronic and Manufacturing Engineering*, **5**.

[11] ASHRAE Fundamentals Handbook, SI, Chapter 27, 1997.

[12] Department of Mechanical Engineering, Technical University of Denmark, Nils Koppels Allé, Building402, DK-2800 Kgs. Lyngby, DENMARK, 2001. http://www.en.ipu.dk/Indhold/refrigeration-and-energy-technology/downloads.aspx

[13] Dincer, I. (2004) Thermal Energy Storage. *Encyclopedia of Energy*, **6**, 14.

[14] Habeebullah, B.A. (2006) Economic Feasibility of Thermal Energy Storage Systems: Application to Al-Haram Grand Holy Mosque Air Conditioning Plant. *JKAU: Eng. Sci.*, **16**, 55-82.

Journal of Electronics Cooling and Thermal Control, 2017, 7, 63-77
http://www.scirp.org/journal/jectc
ISSN Online: 2162-6170
ISSN Print: 2162-6162

# Fabrication and Characterization of PLD-Grown Bismuth Telluride ($Bi_2Te_3$) and Antimony Telluride ($Sb_2Te_3$) Thermoelectric Devices

**Ibrahim M. Abdel-Motaleb*, Syed M. Qadri**

Department of Electrical Engineering, Northern Illinois University, DeKalb, IL, USA
Email: *ibrahim@niu.edu

**How to cite this paper:** Abdel-Motaleb, I.M. and Qadri, S.M. (2017) Fabrication and Characterization of PLD-Grown Bismuth Telluride ($Bi_2Te_3$) and Antimony Telluride ($Sb_2Te_3$) Thermoelectric Devices. *Journal of Electronics Cooling and Thermal Control*, **7**, 63-77.
https://doi.org/10.4236/jectc.2017.73006

**Received:** May 23, 2017
**Accepted:** July 18, 2017
**Published:** July 21, 2017





## Abstract

We report on the fabrication and characterization of multi-leg bismuth telluride ($Bi_2Te_3$) and antimony telluride ($Sb_2Te_3$) thermoelectric devices. The two materials were deposited, on top of $SiO_2$/Si substrates, using Pulsed Laser Deposition (PLD). The $SiO_2$ layer was used to provide insulation between the devices and the Si wafer. Copper was used as an electrical connector and a contact for the junctions. Four devices were built, where the $Bi_2Te_3$ and $Sb_2Te_3$ were deposited at substrate temperatures of 100˚C, 200˚C, 300˚C and 400˚C. The results show that the device has a voltage sensitivity of up to 146 μV/K and temperature sensitivity of 6.8 K/mV.

## Keywords

Thermoelectric Devices, Bismuth Telluride, $Bi_2Te_3$, Antimony Telluride, $Sb_2Te_3$, Pulsed Laser Deposition, PLD, Seebeck Effect

## 1. Introduction

Thermoelectric devices can convert heat to electrical power and vice versa. These devices can be used for many applications, such as micro-cooling and micro-heating. The devices can also be used for converting wasted heat energy from factories, plants, and automobiles to electrical power. Micro-heating and cooling and electrical current generation can be attractive for applications such as powering biomedical sensors, cooling integrated circuits, or operating micro-electromechanical systems (MEMS) devices and sensors.

Thermoelectric devices can be characterized by measuring several parameters that correlate the electrical signals (current and voltage) to the temperature difference. The first parameter used to characterize materials and devices is Seebeck

coefficient. This coefficient relates the difference in voltage, $\Delta V$, to the difference in temperatures, $\Delta T$, between two points [1] [2]. In this case, Seebeck coefficient is a characteristic of the materials. Seebeck coefficient, $S$, can be expressed as:

$$S = -\Delta V/\Delta T \tag{1}$$

For a device composed of two dissimilar materials ($A$ and $B$) forming two junctions at their ends, Seebeck coefficient relates $\Delta V$ and $\Delta T$ of the junctions. Hence,

$$V = \left(S_A - S_B\right)\Delta T, \tag{2}$$

where $S_A$ and $S_B$ are Seebeck coefficients for materials $A$ and $B$, respectively. In this case, the effective Seebeck coefficient for the device is

$$S = S_A - S_B \tag{3}$$

To characterize the thermoelectric performance, Altenkirch found that a dimensionless figure of merit can provide a better indication of the thermoelectric quality of a material than Seebeck or Peltier effects [1] [2] [3]. This figure of merit, ZT, can be expressed as

$$\mathrm{ZT} = \frac{\sigma S^2 T}{k}, \tag{4}$$

where $\sigma$, $S$, and $k$ are the electrical conductivity, Seebeck coefficient, and thermal conductivity of the material, respectively. From Equation (3), it can be observed that a material with good thermoelectric properties should have high $\sigma$, high $S$, and low $k$.

For a device built using $n$-type and $p$-type materials, the figure of merit, ZT, can be obtained from the following Equation [1]:

$$\mathrm{ZT} = \frac{\left(S_p - S_n\right)^2 T}{\left[\left(\rho_n k_n\right)^{0.5} + \left(\rho_p k_p\right)^{0.5}\right]^2}, \tag{5}$$

where $S_n$, $\rho_n$, and $k_n$ are the Seebeck coefficient, the resistivity, and the thermal conductivity of the $n$-type material, respectively. Similarly, $S_p$, $\rho_p$, and $k_p$ are the Seebeck coefficient, the resistivity, and the thermal conductivity for the $p$-type material, respectively. As indicated by Equation (3), for thermoelectric devices, the Seebeck coefficient of the device is $S = S_p - S_n$.

There are many different materials that can be used to build thermoelectric devices. Chalcogenides group is one type of these thermoelectric materials. They are materials that contain one or more elements such as S, Se or Te as a substantial constituent, such as $CsBi_4Te_6$, $Tl_2SnTe_5$ and $Tl_2GeTe_5$, PbTe, and $ZfTe_5$ [4] [5] [6] [7]. Skutterudites, such as $(Ce_yFe_{1-y})_xCo_{4-x}$, form another set of materials. It was reported that this material has a figure of merit of 1.4 at 1000 K [1]. Half Heusler alloys, such as $Zr_{0.5}Hf_{0.5}NiSb_xSn_{1-x}$, were investigated and found to have $S$ = 10 μ/K, at 50 K [8]. Clathrates materials, such as $Eu_8Ga_{16}Ge_{30}$ and $Sr_8Ga_{16}Ge_{30}$, were found to have low thermal conductivity, which results in high figure of merit [9] [10]. Alloys of Te-Ag-Ge-Sb, which is referred to as TAGS,

can provide ZT > 1 [11] [12]. $Ca_3Co_4O_9$ and single-crystal $NaCo_2O_4$ achieved Seebeck coefficient value of 130 and 100 μV/K, respectively [13] [14].

One of the most promising materials for thermoelectric application is Bismuth telluride ($Bi_2Te_3$) and Antimony telluride ($Sb_2Te_3$) [15]. $Bi_2Te_3$ is a natural *n*-type material while $Sb_2Te_3$ is a natural *p*-type material [16]. These materials can be grown using many growth techniques such as Chemical Vapor Epitaxy (CVD), sputtering, Molecular Beam Epitaxy (MBE), among other techniques. Shaik and Abdel-Motaleb have grown $Bi_2Te_3$ and $Sb_2Te_3$ using Pulsed Laser Deposition (PLD) technique [17]. They have also investigated their electrical and optical characteristics [18] [19]. They have shown that good quality of polycrystalline materials of $Bi_2Te_3$ and $Sb_2Te_3$ can be grown using PLD.

In this paper, we designed and fabricated thermoelectric devices using PLD-grown 4-pair legs of *n*-$Bi_2Te_3$ and *p*-$Sb_2Te_3$. The thermoelectric properties of the materials and the devices are investigated. To the best of our knowledge, there is very few published report about the fabrication of a multi-leg, PLD-grown $Bi_2Te_3$ and $Sb_2Te_3$ thermoelectric devices. In fact, we could not identify one credible report. Therefore, we believe that this study will advance the state of the art of this area.

## 2. Device Design

The thermoelectric device consists of an *n*-type and a *p*-type material connected electrically in series and thermally in parallel. The materials used in this device are *n*-type $Bi_2Te_3$ and *p*-type $Sb_2Te_3$, with copper acting as the metal contact between the two materials. The devices were built on a 3-inch p-Si wafer, with 3000˚A of thermally grown $SiO_2$ on top [20]. The $SiO_2$ is used just for isolating the devices from the *p*-Si wafer. The dimensions of each area of the $Bi_2Te_3$ and $Sb_2Te_3$ are 0.4 inch × 0.12 inch. Both materials have 8 regions connected with copper contacts as shown in **Figure 1(a)**. In this figure, the red is $Bi_2Te_3$, the blue

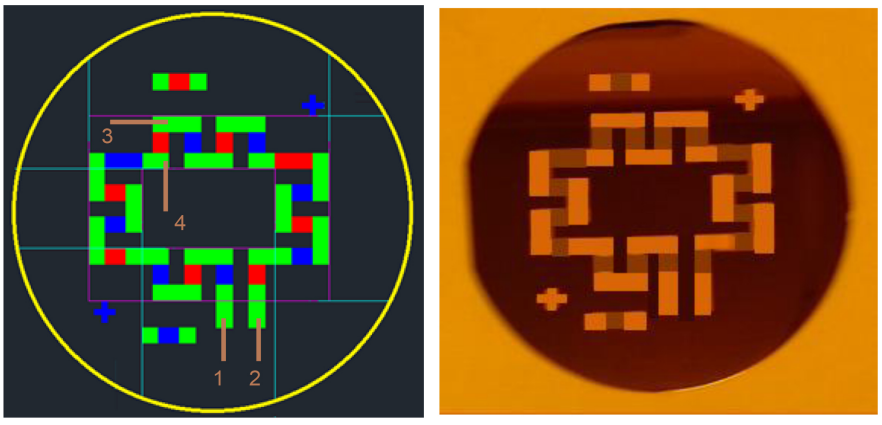


(a) (b)

**Figure 1.** The thermoelectric device. (a) The masks for the tree layers: the red is for the $Bi_2Te_3$, the blue is for $Sb_2Te_3$, and the green is for the copper metal. (b) A photograph of the device after fabrication.

is for $Sb_2Te_3$ and the green color depicts and copper metal. The dimensions for the copper are roughly 0.34 inches × 0.12 inches.

$Bi_2Te_3$ and $Sb_2Te_3$ were grown using the PLD technique. The copper connections were deposited using the electron beam evaporation technique. Three different shadow masks for $Bi_2Te_3$, $Sb_2Te_3$ and the copper were designed and manufactured for the use in building the devices; see **Figure 1(a)**. The finished thermoelectric device is shown in **Figure 1(b)**.

## 3. Material Deposition

$Bi_2Te_3$ and $Sb_2Te_3$ were deposited using Neocera-PLD system [21]. After loading the substrate and mounting the targets for the two materials, the turbo pump was turned on to reduce the pressure to the level of $10^{-6}$ Torr. The substrate temperature was maintained to the set value using a 3-inch heater. The heater is capable of reaching a maximum temperature of 850˚C. The deposition of $Bi_2Te_3$ and $Sb_2Te_3$ was carried out in Argon atmosphere. In this study, four devices were fabricated by depositing these materials at substrate temperatures of 100˚C, 200˚C, 300˚C, and 400˚C. The deposition targets used in the PLD system are 99.999% pure hot pressed $Bi_2Te_3$ and $Sb_2Te_3$ with a diameter of 1-inch and a thickness of 0.125-inch each.

After the chamber was pumped down to about $5 \times 10^{-6}$ Torr, Ar gas was admitted to increase the chamber pressure to the desired deposition pressure of 7.5 mTorr. The substrate temperature increased from room temperature to the required temperature by ramping the heater at 10˚C/minute. KrF laser was applied to the target for 2 hours for a total of 72,000 pulses. The laser beam parameters were set to the following values: incident angle equal 45˚, frequency equal 10 Hz, and energy equal 250 mJ. The targets were set to rotate during the deposition in order to reduce exfoliation.

For each device, both $Bi_2Te_3$ and $Sb_2Te_3$ were deposited at the same substrate temperature. During the deposition, the substrate was covered with its respective shadow mask to form the desired device geometry. Copper metal contacts were deposited using the electron beam evaporation technique and patterned using the shadow mask designed for this purpose.

## 4. Material Characterization

Dektak profilometer was used to measure the thickness of the deposited films. With a vertical resolution of ~5 A. The average thickness was found to be 400 μm for all films, as intended.

The surface morphology of $Bi_2Te_3$ and $Sb_2Te_3$ films were characterized using HITACHI S-4500 Scanning Electron Microscope (SEM). The SEM images of the device were obtained by firing the electron beam at 3 kV. Images with magnification of 2.5 K were taken for $Bi_2Te_3$ and $Sb_2Te_3$ films deposited at the different deposition temperature, as shown in **Figure 2** and **Figure 3**.

$Bi_2Te_3$ deposited at 100˚C was found to be rough with irregular formation of

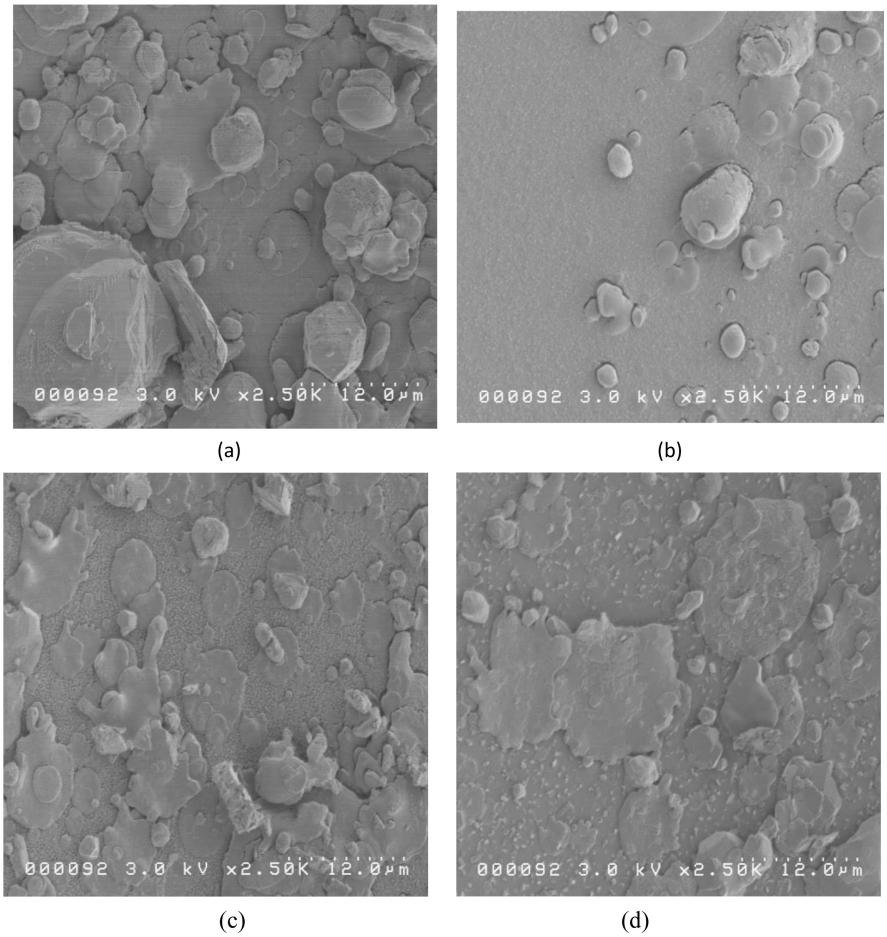


**Figure 2.** SEM images of $Bi_2Te_3$ films with magnification of 2.5 K for films deposited at substrate temperature of (a) 100˚C (b) 200˚C (c) 300˚C (d) 400˚C.

grains. The films deposited at 200˚C were found to have smoother surfaces compared to other films. For the higher temperature substrates, $Bi_2Te_3$ surfaces became rough again with large sizes of island structures. The roughness can be attributed to the high substrate temperatures that caused the grains to over grow and induce roughness [2]. Over growth could be due to the combination of small grains to from lager grains, by a process called secondary recrystallization [16]. However, for $Sb_2Te_3$ films, we found that there was not much difference seen between films deposited at 200˚C and 300˚C.

## 5. Measurement of Effective Seebeck Coefficient or Voltage Sensitivity

To obtain the effective Seebeck coefficient for a device, Seebeck coefficients for the constituent materials ($Bi_2Te_3$ and $Sb_2Te_3$) should be known first. The effective Seebeck coefficient for the device can then be calculated from Equation (3). Another way to obtain the effective Seebeck coefficient for the entire device is to measure it experimentally. This requires that both voltage and temperature differences be measured across the device junction. In our case, we do not have a

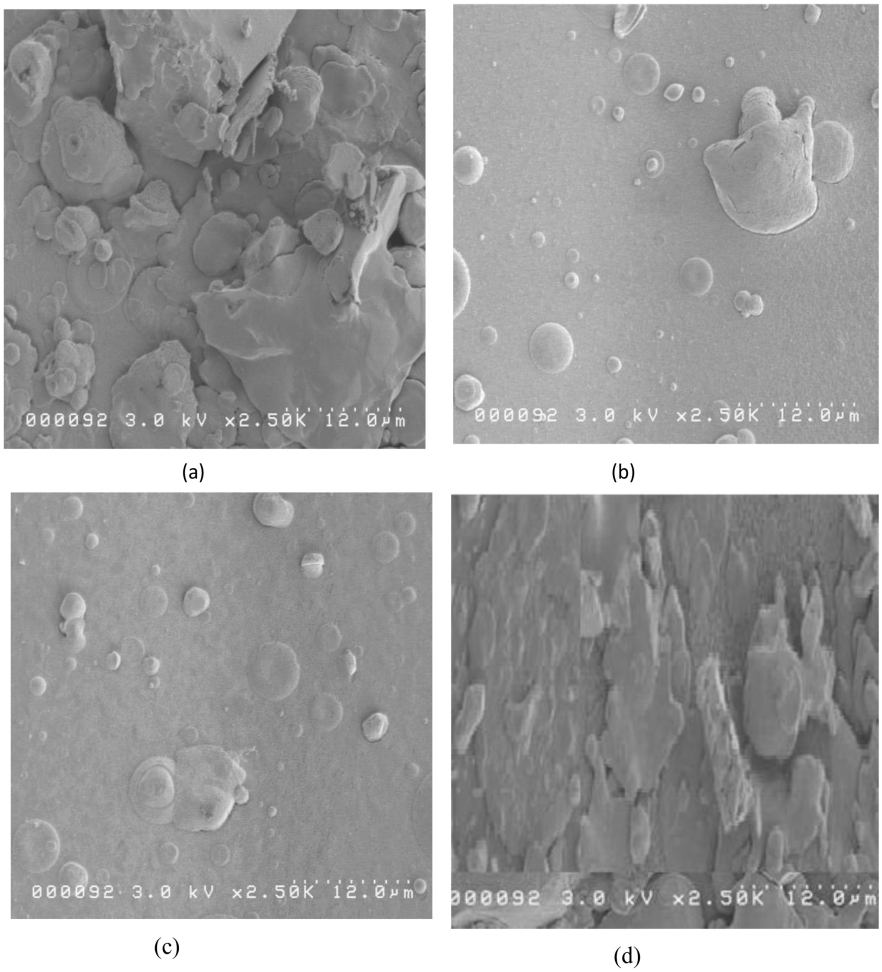


**Figure 3.** SEM images of $Sb_2Te_3$ films with magnification of 2.5 K for films deposited at substrate temperature of (a) 100˚C (b) 200˚C (c) 300˚C (d) 400˚C.

simple one junction device, but rather a more complicated multi-leg device, which requires a more elaborate technique.

In our case, the effective Seebeck coefficient was measured by applying a voltage across points 1 and 2 and measuring the temperature difference between points 3 and 4. Points 1, 2, 3, and 4 are indicated in **Figure 1(a)**. It should be noted that points 1 and 2 are chosen for voltage application because they are the input ports of the device, where the legs are electrically connected in series. On the other hand the temperature difference was measured across junctions 3 and 4. It should be noted that the temperature difference can be measured across any two junctions, and this would still represent the temperature difference across the entire device. This is true because the device legs are thermally connected in parallel, and the temperature difference across any junctions is the same.

In our case, the voltage was supplied using a high precision voltage supply and measured using high resolution voltmeter. The temperature difference, $\Delta T$, was measured using SA1-K (Chromega-Alomega) type thermocouple. This thermocouple can measure temperatures from −60˚C to 175˚C continuously with a

time response of 0.3 seconds. This thermocouple has a silicon based cement adhesive attached to a polyimide adhesive pad. Two thermocouples were used for measuring the temperature across the junctions. One lead of the thermocouple was attached to junction 3 using the adhesive pad, while the other lead was connected to the thermal read out using a connector. After applying the desired voltage across points 1 and 2, the temperature of junction 3 was measured from the reading of the thermal read out. Similarly the temperature of junction 4 was measured using the other thermocouple. The difference between the readings of the two thermal readouts gave the temperature difference across junctions, 3 and 4.

As shown in Figure 4, the device with a material deposition temperature of 100˚C has temperature difference ($\Delta T$) varied from 0 to 3 K for an applied voltage from 0 to 0.25 mV. The temperature difference remained almost constant when the voltage increased beyond this value. This may be due to the heat loss, resulting from thermal leakage to the substrate and radiation to the surroundings. This may also be due to the fact that none of the junctions were maintained at constant room temperature using a heat sink. As a result, the temperatures at

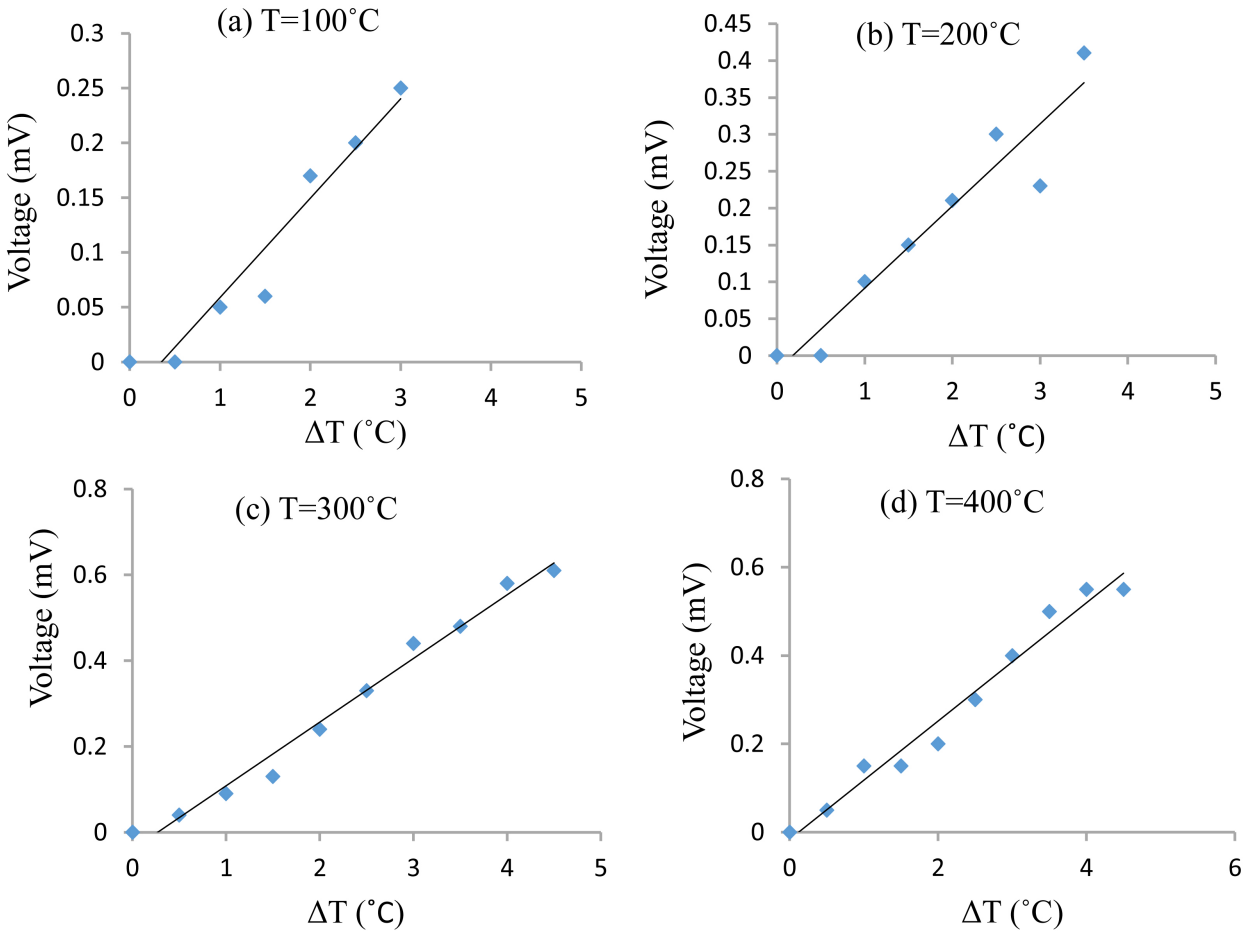


Figure 4. Temperature difference between the junctions when voltage is applied at the terminals of device with substrate temperatures of (a) 100˚C (b) 200˚C (c) 300˚C (d) 400˚C.

both the junctions changed simultaneously reducing the temperature difference between the junctions. However, this effect would not be prominent, if the applied voltage is kept low. For this reason, the applied voltage was maintained at low values to ensure accurate results.

For the device built with material deposition temperature of 200˚C, $\Delta T$ increased to 3.5 K when a voltage of 0.41 mV was applied. For the device built at 300˚C, $\Delta T$ increased to 4.5 K when a voltage of 0.61 mV was applied. Finally for the device deposited at 400˚C, $\Delta T$ increased to 4.5 K when 0.55 mV was applied at the terminals 1 and 2. Similar to the first device, no further increase in $\Delta T$ was observed when the voltages were increased beyond these values.

The ratio of the voltage applied to the temperature difference gives the effective Seebeck coefficient for the device, or. This ratio is the slope of the graph in Figure 4. From this Figure, it can be shown that the effective Seebeck coefficients are 93 μV/K, 100 μV/K, 146 μV/K and 132 μV/K for the devices with deposition temperatures of 100˚C, 200˚C, 300˚C and 400˚C, respectively. It was observed that the effective Seebeck coefficient increases with the increase of the substrate temperature, reaching a maxima at 300˚C, then decreases after that. The increase could be due to the decrease in the thermal conductivity of the materials at high deposition temperatures [22]. The subsequent decrease could be due to the excessive increase in the resistivity of $Bi_2Te_3$ which leads to the increase of the voltage drop outside the junction, reducing the effective $\Delta V$. Kimi and Oh reported the fabrication of electrodeposited 196 pairs of $Bi_2Te_3$ and $Sb_2Te_3$ thin film legs thermopile [23]. They controlled the temperature difference of the thermopile and measured the voltage difference. When the temperature difference was set to 14˚C, a maximum sensitivity of 57.5 mV/K was obtained. This high value of the voltage sensitivity is attributed to the large number of pairs of legs and the size of device layers.

## 6. Thermal Conductivity

There are various methods used for the measurement of thermal conductivity of thin films. Among these methods are the thermal conductance, thermal diffusive, thermos-reflectance, the laser flash, and the $3\omega$ method [24] [25]. In this work, the thermal conductivity values were taken from the literatures [24] [26]. The thermal conductivity for $Bi_2Te_3$ for different growth temperatures are shown in Table 1. For $Sb_2Te_3$, thermal conductivity values for PLD-grown films at the

Table 1. Thermal conductivity values of $Bi_2Te_3$.

| Substrate temperature | Thermal conductivity of $Bi_2Te_3$ ($Wm^{-1}\cdot K^{-1}$) [24] [26] | Resistivity of $Bi_2Te_3$ (μΩ·m) (This work) | Resistivity of $Sb_2Te_3$ (μΩ·m) (This work) |
|---|---|---|---|
| 100˚C | 1.75 | 40 | 24 |
| 200˚C | 1.5 | 44 | 17.68 |
| 300˚C | 0.9 | 68 | 16 |
| 400˚C | 0.8 | 84 | 15 |

same growth temperatures are hard to find in the literature. Therefore, an average value of thermal conductivity of 1.63 $Wm^{-1}\cdot K^{-1}$ was used for all films of $Sb_2Te_3$ [27].

## 7. Electrical Conductivity

The measured electrical parameters of $Bi_2Te_3$ and $Sb_2Te_3$ films, obtained using the four point probe technique, are shown in Figures 5(a)-(c). The Figure shows

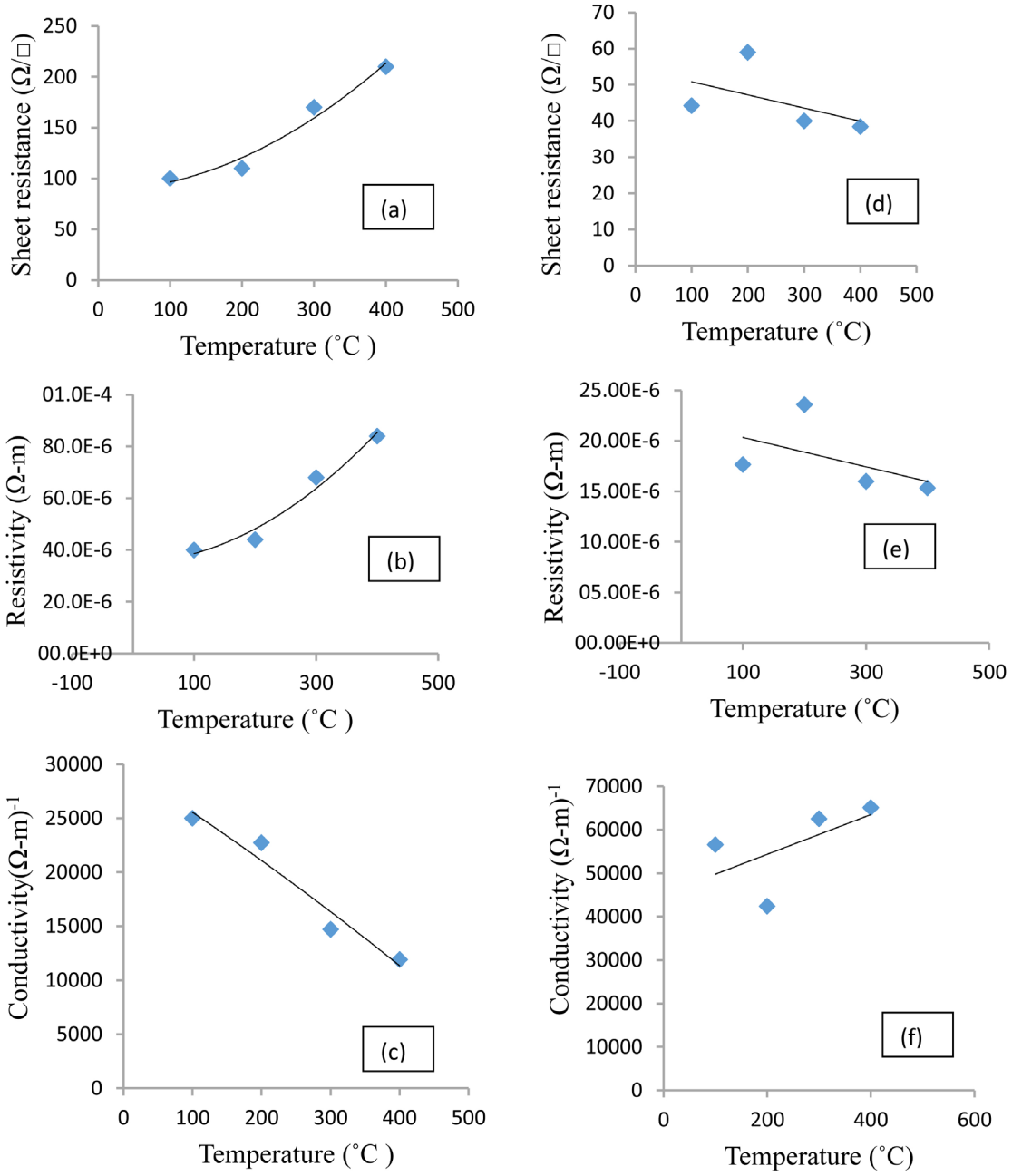


Figure 5. Electrical Parameters for $Bi_2Te_3$ (a) Sheet Resistance (b) Resistivity (c) Electrical conductivity with temperature. Electrical Parameters for $Sb_2Te_3$ (d) Sheet Resistance (e) Resistivity (f) Electrical conductivity with temperature.

the effect of substrate temperature on the sheet resistance, resistivity and the electrical conductivity. The value of the sheet resistance for $Bi_2Te_3$ was found to increase with the substrate temperature, with a maximum value of 210 (Ω/□) at 400˚C. When the substrate temperature increases, grains over grow resulting in increasing the roughness and irregularities in the film. This results in increasing the sheet resistance of the film. This increase may be due to carrier scattering at the rough boundaries of the grains, which increases with the growth temperature [18]. Consequently, the resistivity increases and the conductivity decreases with increasing the substrate temperature. These findings have also been observed in references [18] [28].

The sheet resistance was measured for $Sb_2Te_3$ films using the four point probe too. The measured values of the sheet resistance, resistivity and the electrical conductivity, as a function of the substrate growth temperature, are shown in **Figures 5(d)-(f)**. As shown in the Figure, the resistivity of the films, and consequently the sheet resistance, changes only by about ±15% from the average value. Therefore, the sheet resistance and resistivity can be assumed to be almost constant with temperature, even though they have decreasing values. The conductivity will behave accordingly.

The resistivity of $Sb_2Te_3$ films behaves differently from $Bi_2Te_3$ films, where the resistivity remains almost constant with growth temperature. This behavior can be attributed to the finding that the grain size of PLD-grown $Sb_2Te_3$ films does not change with the temperature growth. Hence the level of scattering of the carriers at the grain boundaries is the same for all samples. The same behavior has been observed and reported by in references [18] [29].

## 8. Figure of Merit and Power Factor

To the best of our knowledge there is no published report on the figure of merit of multi-leg devices built using PLD-grown $Bi_2Te_3$ and $Sb_2Te_3$. However, there are reports of calculated figure of merit when the material thin film is used individually to build the device.

The figure of merit of one pair of p-n legs thermoelectric device can be calculated using Equation (5). The values of the device effective Seebeck coefficient (voltage sensitivity) and $Bi_2Te_3$ and $Sb_2Te_3$ electrical resistivity and thermal conductivity are obtained from Sections 5, 6, and 7 above. The Seebeck values measured are for the entire 4-pair legs device. Since these devices are electrically connected in series, the Seebeck coefficient of one pair of $Bi_2Te_3$ and $Sb_2Te_3$ leg is 25% of the measured value. These values are used in our calculation of the Figure of Merit (ZT) and the Power Factor (PF), shown in **Table 2**. The power factor (PF) measures the performance of the device and can be obtained from the equation $PF = S^2\sigma$. When calculating the PF, the effective resistivity of the two materials becomes $r = r_n + r_p$ and the effective thermal conductivity becomes $k = k_n + k_p$, since the dimensions of the $n$ region is the same as those of the $p$-region [30].

**Table 2.** Performance parameters at different temperatures.

| Substrate temperature (˚C) | Device effective seebeck coefficient (Voltage sensitivity) (μV/K) | Effective electrical resistivity for one pair, r (μΩ·m) | Effective thermal conductivity for one pair, k ($Wm^{-1}\cdot K^{-1}$) | Figure of merit (ZT) measurements at room temperature for one pair | Power factor for one pair $PF = S^2\cdot\sigma$ ($\mu W/K^2\cdot m$) |
|---|---|---|---|---|---|
| 100 | 93 | 84 | 3.38 | $7.586 \times 10^{-4}$ | 8.446 |
| 200 | 100 | 61.68 | 3.13 | 0.001 | 10.133 |
| 300 | 146 | 84 | 2.53 | 0.003 | 20.816 |
| 400 | 132 | 101 | 2.43 | 0.002 | 10.96 |

Table 2 shows the values of ZT and the PF of one pair of legs deposited at different growth temperatures. The two parameters for the device were calculated at room temperature. It can be observed that the figure of merit increases for the substrate temperature until 300˚C and then it decreases for the device with a substrate temperature of 400˚C. The power factor behaves exactly the same way. For devices with growth temperatures at 100˚C, 200˚C and 300˚C, the thermal conductivity of the device was found to decrease with temperature and this is accompanied by an increase in the effective Seebeck coefficient, which results in the increase in the figure of merit and the power factor of the device. The decrease for device built at 400˚C can be attributed to the slight decrease in the electrical conductivity and the effective Seebeck coefficient at that temperature.

The performance of our devices can be enhanced if more pairs of legs are used. Kimi and Oh reported the fabrication of 196 pairs of $Bi_2Te_3$ and $Sb_2Te_3$ thin film legs thermopile using electrodeposition [23]. They reported a voltage sensitivity from 57.5 mV/K for the entire device. However by dividing the reported sensitivity value by 196 (the number of pairs of legs), the value is reduced to 293 μV/K. Our voltage sensitivity values have been affected by the fact that the device was not thermally isolated and without a heat sink. This resulted in the loss of heat due to radiation and thermal conductivity. Our simulation shows that by using a heat sink, the voltage sensitivity will increase by 25% - 200% [31].

Using Seebeck coefficient or voltage sensitivity for all types of thermoelectric devices may not provide an accurate evaluation of the performance of some types of devices. This because a device designed for cooling is different from that built for energy harvesting. The optimum parameters for one type may not be the optimum for another type. Similar to an amplifier, the characteristics for a common base configuration is different from a common emitter configuration. One has high current gain but low voltage gain and the other has higher gain for both.

The devices reported here use politer effect, not Seebeck effect. The input to our device is voltage and the output is temperature difference. Hence the device sensitivity should be temperature sensitivity $\Delta T/\Delta V$, not voltage sensitivity, which is related to Seebeck Coefficient. To differentiate between the two para-

meters, let us call the voltage sensitivity $S_V$ and the temperature sensitivity $S_T$. Let us now compare the device reported in [23] by Kimi and Oh, with our device. For our device the highest value for $S_V$ is 146 μV/K for the 4 pairs of legs device fabricated at 300˚C. This means for one leg, $S_V$ = 36.5 μV/K. For Kimi and Oh device the maximum $S_V$ = 57.5 mV/K for 196 pairs. This means for a pair of legs, $S_V$ = 293 μV/K, which is higher than our device. However, if we compare the temperature sensitivity for one pair, we will find that our device has $S_T$ = 27.4 K/mV compared with Kimi and Oh device, where $S_T$ = 3.4 K/mV. This means our device is geared to obtain higher temperature sensitivity, since it is used for cooling/heating based on politer effect. On the other hand, Kimi and Oh device is geared for energy harvesting, hence it should have higher voltage sensitivity. Temperature sensitivity can be obtained from the voltage sensitivity where $S_T = 1/S_V$.

## 9. Conclusions

In conclusion, we report on the design and fabrication of thermoelectric devices composed of 4-pairs of legs of PLD grown *n*-$Bi_2Te_3$ and *p*-$Sb_2Te_3$ thin films. $Bi_2Te_3$ and $Sb_2Te_3$ are simple compounds, easy to synthesize and deposit, have very high conductivity, and are naturally doped. These advantages make the cost of building devices much lower than the more complex alloys.

Our study shows that these multi-leg devices have the performance that makes them attractive for cooling/heating devices. However, these devices can even provide much higher performance, if the geometry and fabrication process are optimized to serve the application targeted. The devices fabricated achieved a maximum effective Seebeck coefficient of 146 μV/K, a figure of merit of 0.03, and a power factor of 20.8 μW/m·K$^2$.

Although the convention is to use Seebeck coefficient, the power factor, and the figure of merit to characterize any device, we believe that such parameters should not be used universally for all thermoelectric devices. The performance of a device used for energy harvesting, can be evaluated using the voltage sensitivity, $S_V = \Delta V/\Delta T$. However, devices used for cooling/heating application should use temperature sensitivity $S_T = \Delta T/\Delta V$, instead. Since the reported devices are designed for cooling/heating applications, temperature sensitivity represents the best indication of the device performance. For one pair of legs, our device exhibited a max $S_T$ of 27.4 K/mV compared with 3.4 K/mV for the device reported by Kimi and Oh. However, our devices have lower voltage sensitivity of 36.5 μV/K compared with 293 μV/K for the device of Kimi and Oh for one pair of legs. These results support our claim that cooling and heating devices, such as ours, should be optimized to achieve higher temperature sensitivity, while energy harvesting devices should be optimized to obtain higher voltage sensitivity.

The performance of this device can be enhanced several fold, if superlattice layers are used [32]. The enhancement in these materials is mainly attributed to the controlling of the transport of phonons and photons in the super lattice. In

order to understand and confirm the results obtained by this study, a theoretical study, such as multi-physics numerical analysis, may need to be conducted [31].

## Acknowledgements

The authors would like to acknowledge Northern Illinois University and its Microelectronic Research and Development Laboratory (MRDL) for supporting this work.

## References

[1] Willfahart, A. (2014) Screen Printed Thermoelectric Devices. Linköpings Universitet, SE-60174 Norrköping.

[2] Tritt, T.M. (2002) Thermoelectric Materials: Principles, Structure, Properties, and Applications. *Encyclopedia of Materials*: *Science and Technology*, 1-11.

[3] Nolas, G.S., Sharp, J. and Goldsmid, J. (2001) Thermoelectrics: Basic Principles and New Materials Developments. Springer, New York City. https://doi.org/10.1007/978-3-662-04569-5

[4] Chung, D.-Y., *et al.* (2000) $CsBi_4Te_6$: A High-Performance Thermoelectric Material for Low-Temperature Applications. *Science*, **287**, 1024-1027. https://doi.org/10.1126/science.287.5455.1024

[5] Sharp, J.W., Sales, B.C., Mandrus, D.G. and Chakoumakos, B.C. (1999) Thermoelectric Properties of $Tl_2SnTe_5$ and $Tl_2GeTe_5$. *Applied Physics Letters*, **74**, 21.

[6] Dughaish, Z.H. (2002) Lead Telluride as a Thermoelectric Material for Thermoelectric Power Generation. *Physica B*: *Condensed Matter*, **322**, 205-223. https://doi.org/10.1016/S0921-4526(02)01187-0

[7] Littleton IV, R.T., Tritt, T.M., Korzenski, M., Ketchum, D. and Kolis, J.W. (2001) Effect of Sb Substitution on the Thermoelectric Properties of the Group IV Pentatelluride Materials $M_{1x}Y_xTe_5$ (M¼Hf, Zr and Ti). *Physical Review B*, **64**, 121104-121107.

[8] Uher, C., Yang, J., Hu, S., Morelli, D.T. and Meisner, G.P. (1999) Transport Properties of Pure and Doped MNiSn, M= (Zr, Hf). *Physical Review B*, **59**, 8615-8621.

[9] Nolas, G.S., Cohn, J.L., Slack, G.A. and Schujman, S.B. (1998) Semiconducting Ge Clathrates: Promising Candidates for Thermoelectric Applications. *Applied Physics Letters*, **73**. https://doi.org/10.1063/1.121747

[10] Meng, J.F., Chandra Shekar, N.V., Badding, J.V. and Nolas, G.S. (2001) Threefold Enhancement of the Thermoelectric Figure of Merit for Pressure Tuned $Sr_8Ga_{16}Ge_{30}$. *Journal of Applied Physics*, **89**.

[11] Snyder, G.J. and Toberer, E.S. (2008) Complex Thermoelectric Materials. *Nature Materials*, **7**, 105-114. https://doi.org/10.1038/nmat2090

[12] Levin, E.M., Bud'ko, S.L. and Schmidt-Rohr, K. (2012) Enhancement of Thermopower of TAGS-85 High-Performance Thermoelectric Material by Doping with the Rare Earth Dy. *Advanced Functional Materials*, **22**, 2766-2774. https://doi.org/10.1002/adfm.201103049

[13] Hu, Y.F., Sutter, E., Si, W.D. and Li, Q. (2005) Thermoelectric Properties and Microstructure of C-Axis-Oriented $Ca_3Co_4O_9$ Thin Films on Glass Substrates. *Applied Physics Letters*, **87**, Article ID: 171912. https://doi.org/10.1063/1.2117615

[14] Terasaki, I., Sasago, Y. and Uchinokura, K. (1997) Large Thermoelectric Power in $NaCo_2O_4$ Single Crystals. *Physical Review B*, *Third Series*, **56**, R12685-R12687.

[15] Skrabek, E.A. and Trimmer, D.S. (1995) Properties of the General TAGS System. In: Rowe, D.M., Ed., *CRC Handbook of Thermoelectrics*, CRC, Boca Raton, 267-275.

[16] Shaikh, M. (2012) Structural, Electrical and Optical Characterization of Bismuth Telluride and Antimony Telluride Thin Films Deposited by Pulsed Laser Deposition. Graduate Thesis, CEET, Northern Illinois University.

[17] Shaik, M. and Abdel-Motaleb, I.M. (2013) Effect of Substrate Temperature on PLD Grown Thin Film $Bi_2Te_3$ and $Sb_2Te_3$. *IEEE EIT Conference Proceedings*, Rapid City, 8-11 May 2013.

[18] Shaik, M. and Abdel-Motaleb, I.M. (2013) Investigation of the Electrical Properties of PLD Grown Thin Film $Bi_2Te_3$ and $Sb_2Te_3$. *IEEE EIT Conference Proceedings*, Rapid City, 8-11 May 2013.

[19] Shaik, M. and Abdel-Motaleb, I.M. (2013) Investigation of the Optical Properties of PLD Grown Thin Film $Bi_2Te_3$ and $Sb_2Te_3$. *IEEE EIT Conference Proceedings*, Rapid City, 8-11 May 2013.

[20] Zhang, C. and Najafi, K. (2004) Fabrication of Thick Silicon Dioxide Layers for Thermal Isolation. *Journal of Micromechanics and Microengineering*, **14**, 769-774. https://doi.org/10.1088/0960-1317/14/6/002

[21] Brochure for PLD System. http://www.Neocera.com

[22] Termentzidis, K., Pokropivny, A., Woda, M., Xiong, S.Y., Chumakov, Y., Cortona, P. and Volz, S. (2012) Structure Impact on the Thermal and Electronic Properties of Bismuth Telluride by Ab-Initio and Molecular Dynamics Calculations. *Journal of Physics*: *Conference Series*, **395**, Article ID: 012114. https://doi.org/10.1088/1742-6596/395/1/012114

[23] Kimi, M.-Y. and Oh, T.-S. (2011) Processing and Thermoelectric Performance Characterization of Thin-Film Devices Consisting of Electrodeposited Bismuth Telluride and Antimony Telluride Thin-Film Legs. *Journal of Electronic Materials*, **40**, 759-764. https://doi.org/10.1007/s11664-011-1562-8

[24] Wang, H. and Sen, M. (2009) Analysis of the 3-Omega Method for Thermal Conductivity Measurement. *International Journal of Heat and Mass Transfer*, **52**, 2102-2109. https://doi.org/10.1016/j.ijheatmasstransfer.2008.10.020

[25] Tsukada, T., Fukuyama, H. and Kobatake, H. (2007) Determination of Thermal Conductivity and Emissivity of Electromagnetically Levitated High-Temperature Droplet Based on the Periodic Laser-Heating Method: Theory. *International Journal of Heat and Mass Transfer*, **50**, 3054-3061. https://doi.org/10.1016/j.ijheatmasstransfer.2006.12.026

[26] Mavrokefalos, A., Moore, A.L., Pettes, M.T., Shi, L., Wang, W. and Li, X. (2009) Thermoelectric and Structural Characterizations of Individual Electrodeposited Bismuth Telluride Nanowires. *Journal of Applied Physics*, **105**, Article ID: 104318. https://doi.org/10.1063/1.3133145

[27] Choi, J.H., Young, D., Park, S.J., Choo, B.K. and Jang, J. (2003) Temperature Dependence of the Growth of Super-Grain Polycrystalline Silicon by Metal Induced Crystallization. *Thin Film Solids*, **427**, 289-293. https://doi.org/10.1016/S0040-6090(02)01150-1

[28] Chen, C.-L., Chen, Y.-Y., Lin, S.-J., Ho, J.C., Lee, P.-C., Chen, C.-D. and Harutyunyan, S.R. (2010) Fabrication and Characterization of Electrodeposited Bismuth Telluride Films and Nanowires. *The Journal of Physical Chemistry C*, **114**, 3385-3389. https://doi.org/10.1021/jp909926z

[29] Pradyumnan, P.P. and Swathikrishnan (2010) Thermoelectric Properties of $Bi_2Te_3$

and $Sb_2Te_3$ and Its Bilayer Thin Films. *Indian Journal of Pure & Applied Physics*, **48**, 115-120.

[30] Lee, H., Attar, A. and Weera, S. (2015) Performance Prediction of Commercial Thermoelectric Cooler Modules Using the Effective Material Properties. *Journal of Electronic Materials*, **44**, 2157-2165. https://doi.org/10.1007/s11664-015-3723-7 http://homepages.wmich.edu/~leehs/ME695/Thermoelectric%20Coolers%20for%20class.pdf

[31] Abdel-Motaleb, I. and Qadri, S. Multi-Physics Numerical Simulation of Thermoelectric Devices. (In Preparation)

[32] Venkatasubramanian, R., Siivola, E., Colpitts, T. and O'Quinn, B. (2001) Thin-Film Thermoelectric Devices with High Room-Temperature Figures of Merit. *Nature*, **413**, 597-602.

Journal of Electronics Cooling and Thermal Control, 2017, 7, 78-89
http://www.scirp.org/journal/jectc
ISSN Online: 2162-6170
ISSN Print: 2162-6162

# Compact Thermal Management Device Using Electrocaloric Effect

**Yuchen Xi**

High School Affiliated to Fudan University, Shanghai, China
Email: Lawrence_xi13@126.com

**How to cite this paper:** Xi, Y.C. (2017) Compact Thermal Management Device Using Electrocaloric Effect. *Journal of Electronics Cooling and Thermal Control*, **7**, 78-89.
https://doi.org/10.4236/jectc.2017.73007

**Received:** June 16, 2017
**Accepted:** September 22, 2017
**Published:** September 25, 2017



## Abstract

The electrocaloric effect (ECE) is defined as the fact that the temperature of dielectric material changes, when an electric field is applied to or removed from the material [1]. It might be a possible solution for the increasing energy consumption for thermal management because of its high effectiveness. Previous research on the ECE has investigated several possible methods to build a model based on ECE and feasibilities to increase the efficiency of the model. But there has been no study on all the factors that may affect the performance of the device. Thus, in this paper, we designed a cooling device based on ECE and simulated it by using the control variates method showing that a high efficiency can be reached through stated model.

## Keywords

Thermal Management, The Electrocaloric Effect, Simulation, Control Variables

## 1. Introduction

Significant amount of energy has been used for thermal management all over the world presently. In common American families, more than 30% of the power usage is spent on space cooling and refrigeration [1]. If we assume there to be a 10% increase of efficiency in the performance of thermal management applications, 110 terawatt hours of energy would be saved in America in 1 year. This is about the entire energy consumption of Mexico estimated annually [2]. Based on such huge benefits from energy saving, scientists have studied four types of cooling technologies, including the vapor compression system, thermoelectric cooling, magnetocaloric cooling and the electrocaloric cooler [3].

Vapor Compression Refrigeration (VCR) [4], currently the most widely used thermal management technology, was invented about two hundred years ago.

The improvement of efficiency is limited currently. Moreover, it is not environment-friendly because the emission of Chlorofluorocarbons can cause great Ozone depletion, and influence the climate all over the word. Also, the development of this cooling system is restricted by its size. Over the years, there has been little progress in the minimization of such compressors due to many physics problems. Considering that too much energy has been used for thermal management, including but not limited to air conditioning, improvements for cooling technology become more and more important.

Thermoelectric effects have been studied for decades. The Peltier effect is the utilization of the physics thermoelectric cooling [5]. It is defined by the presence of heating or cooling at an electrified junction of two different conductors. With Peltier effect, heat is supposed to be transported from one side of an electrode to the other side with directed motion of charge carriers. One of the most significant advantages of a thermoelectric cooling device is that it can work under many extremely severe conditions. For instance, Thermoelectric coolers and generators have been used in the space. Usually thermoelectric thermal management devices are very simply-built and can be made quite compacted, which VCR system can't solve. However, thermoelectric coolers often suffer from their low efficiency. The fundamental physics requires low thermal conductance and high electric conductance of the materials for high efficiency thermoelectric cooling devices. While for a thermoelectric cooler, these are incompatible requirements, making material exploration for high performance thermoelectric materials challenging.

Magnetocaloric cooling utilizes the thermodynamically reversible magnetocaloric effect (MCE) [5], to transfer heat from cold sources to hot sources in a manner similar to VCR system. Theoretical analyses suggest that compared with the current best air-cooling system, the VCR system, magnetic cooling could have a higher cooling efficiency. However, it is limited by its high magnetic field requirement.

The discovery of the electrocaloric effect (ECE) has offered us a possible solution to the thermal management system efficiency problem [6]. Specifically, variations in the electric field cause change of the dipolar state in the dielectric materials, causing the material to change from a less ordered state to a more ordered state, or *vice versa* when an electric field is removed. The entropy change results in the temperature change. Scientists reported that a temperature change of 12 K can be achieved by tuning the material's composition or introducing higher electric field [7]. This makes it promising to study the ECE, when aiming at designing a system that can increase the efficiency for thermal management.

## 2. Fundamentals of Electrocaloric Effect

In 2004, Zhang predicted a large ECE in ferroelectric P(VDF-TrFE) based polymers. The equation of the ECE is basically derived from the equation of Gibb's free energy.

The derivation is shown below.

$$dG = -SdT - DdE$$

$$dG = \left(\frac{\partial G}{\partial T}\right)_E dT + \left(\frac{\partial G}{\partial E}\right)_T dE$$

$$S = -\left(\frac{\partial G}{\partial T}\right)_E, \; D = -\left(\frac{\partial G}{\partial E}\right)_T$$

$$\frac{\partial G}{\partial T}\frac{\partial G}{\partial E} = \left[\frac{\partial\left(\frac{\partial G}{\partial E}\right)_S}{\partial T}\right]_E = \left[\frac{\partial\left(\frac{\partial G}{\partial T}\right)_E}{\partial E}\right]_T$$

$$\left[\frac{\partial S}{\partial E}\right]_T = \left[\frac{\partial D}{\partial T}\right]_E$$

$$\Delta S = \int_{E1}^{E2}\left(\frac{\partial G}{\partial T}\right)_E dE$$

$$\Delta Q = -\Delta T * \left(C_E * \rho\right), \; \Delta Q = T * \Delta S = -T\int_{E1}^{E2}\left(\frac{\partial D}{\partial T}\right)_E dE$$

$$\Delta T = -\frac{T}{\rho}\int_{E1}^{E2}\frac{1}{C_E}\left(\frac{\partial D}{\partial T}\right)_E dE$$

$G$: Gibbs free energy; $S$: Entropy of material; $C\_E$, $\rho$: Specific heat of material, density of material; $T$: Temperature. $D$: Displacement; $Q$: Heat; $E$: Electric field.

From the derivation of the above equations, it could be seen that temperature change of Electrocaloric materials arises from the entropy change, and is directly related to the displacement under given electric fields. The higher the voltage of the electric field is, the more the temperature changes [8].

## 3. Electrocaloric Cooling Device Design

Theoretically, an ECE refrigerator working under a Carnot cycle can reach the highest possible efficiency, also named as Carnot efficiency. **Figure 1** shows the comparison between VCR and Electrocaloric cooling cycles. As shown in **Figure 1** for Electrocaloric cooling system, it is started with Electrocaloric materials under disordered state. When an external electric filed is applied, the materials tend to be transited into ordered state, which will release the energy in forms of heat during the transition process. After removing the electric filed, the materials will tend to become disorder again and this process requires the materials to absorb the surrounded heat as energy to support the disorder-to-order transition process. In this way, a Electrocaloric cooling system is achieved. And a successful design of Electrocaloric cooling devices should form a similar cycle by utilizing the Electrocaloric temperature changes [6].

Unlike the gaseous refrigerants of VCR systems, all Electrocaloric materials are in solid states. This is an advantage of EC devices, since it yields more compacted sizes, higher energy density, and no friction loss. However, when designing

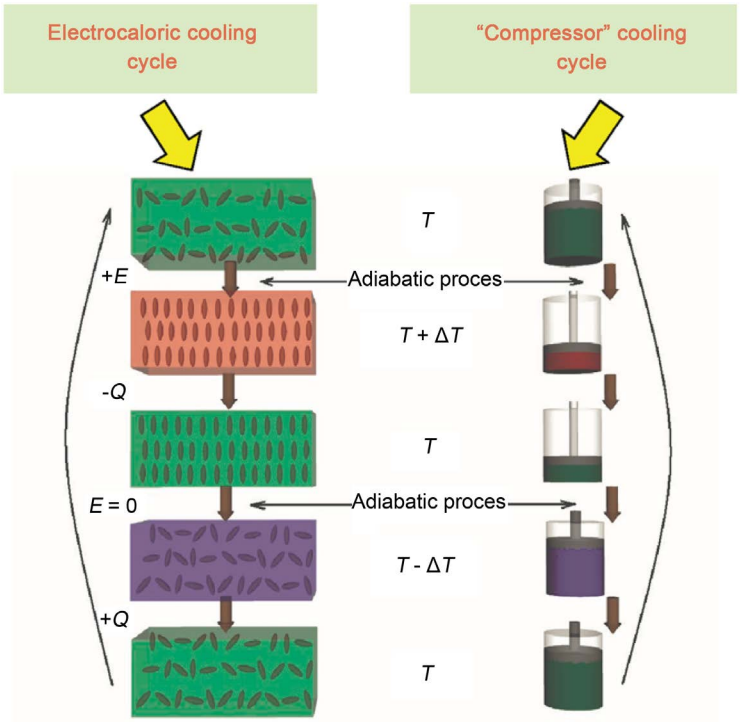


**Figure 1.** Comparison of Electrocaloric cooling cycle and "Compressor" cooling cycle.

a functional EC system, the effeicient thermal transfer between EC materials and thermal ends requires a good thermal switch. A thermal switch is a functional thermal element that changes its thermal conductance in response to changes in thermal loading, and thereby helps maintain a target device or system to stay within desired temperature ranges. When a target device goes over a critical temperature, the switch turns on and dissipates heat to a cold surface. When the target device then returns to an acceptable temperature, the switch turns off. An ideal heat switch should meet the following needs: great on/off ratio, good sensitivity, and low specific heat.

Figure 2 shows the model of the cooling system using the Electrocaloric effect, coupling with a thermal switch that consists of fluid (water with high specific heat capacity as proposed). In this design, the Electrocaloric material's temperature changes alternatively with the application/removal of an external electric field. The water/air gap passes through the Electrocaloric material periodically. By synchronizing the frequency of the Electrocaloric electric field and water/air gap flow, the upper tunnel water is constantly heated and the lower tunnel is constantly cooled. When the water in the tunnel reaches the hot/cold side, heat exchange occurs, and the complete effect sees the heat being pumped from the cold side to hot side, while a directional heat transfer against the temperature gradient is achieved.

In this model, there are several factors that contribute to the device's performance. In the following section, this paper will discuss these factors in details.

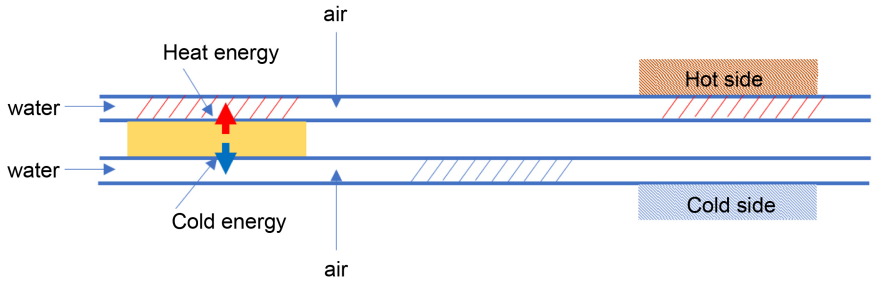


Figure 2. Design of electrocaloric cooling system.

Based on the analyses and modeling results, an optimized design of Electrocaloric cooling device will be presented.

COMSOL 5.2a is used for Multiphysics simulation. The initial parameters are shown as in Table 1.

The initial frequency is set at 1 Hz; thermal conductivity is at 0.12 W/m·K; Electrocaloric temperature change of the EC material is at 5 K; the thickness of water flow is 200 um; the thickness of the EC material is 200 um; and the liquid used for the thermal switch is water. The model illustrated here is a 1-D model. For simplification, let's assume the length and height of the components to be 1cm. To quantify the quality of the model, the power of heat transfer, the change in temperature of the liquid, and the efficiency of the model are considered.

1) Frequency

The relationship between Frequency and the efficiency of EC devices is the first factor to be studied. The Temperature change of working fluids and cooling power are with various frequency as shown in Figure 3. As indicated from the Figure 3, when the frequency increases, the efficiency of the model gradually decreases. When the frequency increases, the temperature change of water decreases. When the frequency increases, the power of the model increases.

The explanation behind these facts may be that when the frequency increases, not enough time will be left for the complete transfer of heat into the liquid, which can cause temperature changes along with efficiency decrease. However, as the frequency increases, the time gap between each transfer decreases, which causes the power of the model to increase. An optimal operation frequency is the result of balanced efficiency, with temperature change and cooling power. After taking all these factors into consideration, an operational frequency of 1 Hz is applied.

2) Thickness of water

The second factors to be studied in this paper is the thickness of the cooling fluid. In this second model, water is used as the cooling fluid for the reason that it has a relatively high thermal conductivity and specific heat. Temperature change of working fluids and cooling power are studied in relation with fluid thickness, as shown in Figure 4. The graphs show that when the thickness of water increases, the efficiency steeply increases at first, then its increment is slowed down. When the thickness of water increases, the temperature change of

**Table 1.** Initial parameters of simulation.

| Name | Expression | Value | Description |
|---|---|---|---|
| l_tube | 20 [um] | 2E−5m | the length of the tube |
| l_water | 200 [um] | 2E−4m | the length of water |
| l_air | 200 [um] | 2E−5m | the length of air |
| dT | 5 [K] | 5 K | change in temperature |
| l_EC | 200 [um] | 2E−4m | the length of EC material |
| thermal conductivity | 0.12 [W/m*K] | 0.12 [W/m*K] | thermal conductivity of EC |

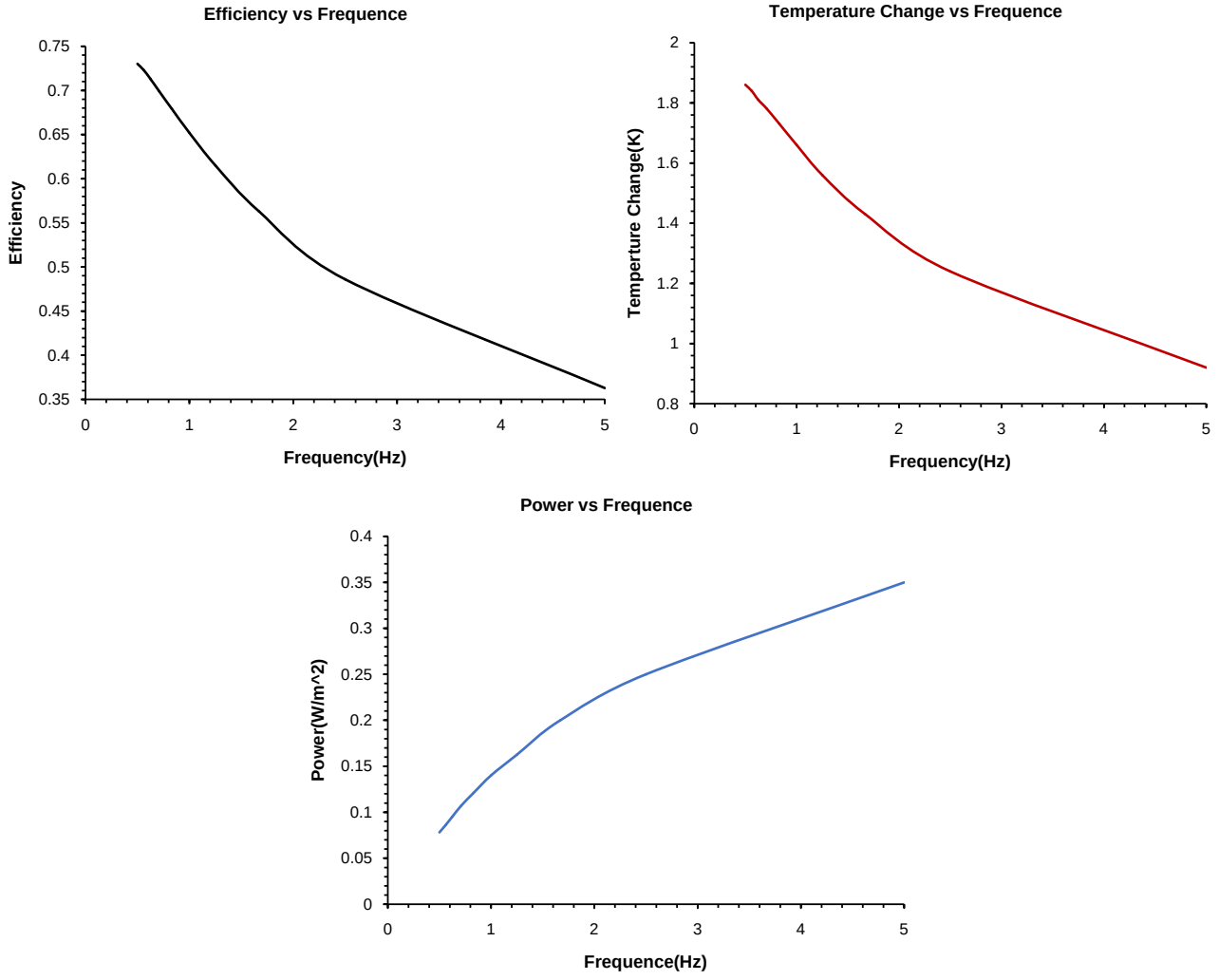


**Figure 3.** Efficiency, temperature change and power change as a function of operation frequency.

water decreases steeply at first, then its decrement is slowed down. When the thickness of water increases, the power of the model increases. This indicates that the increase of water thickness, meaning the increase in the volume of water, increases the efficiency and power, since the more water is implemented the more heat released by the EC material can be absorbed. The temperature change of water will decrease, when the mass of water increases.

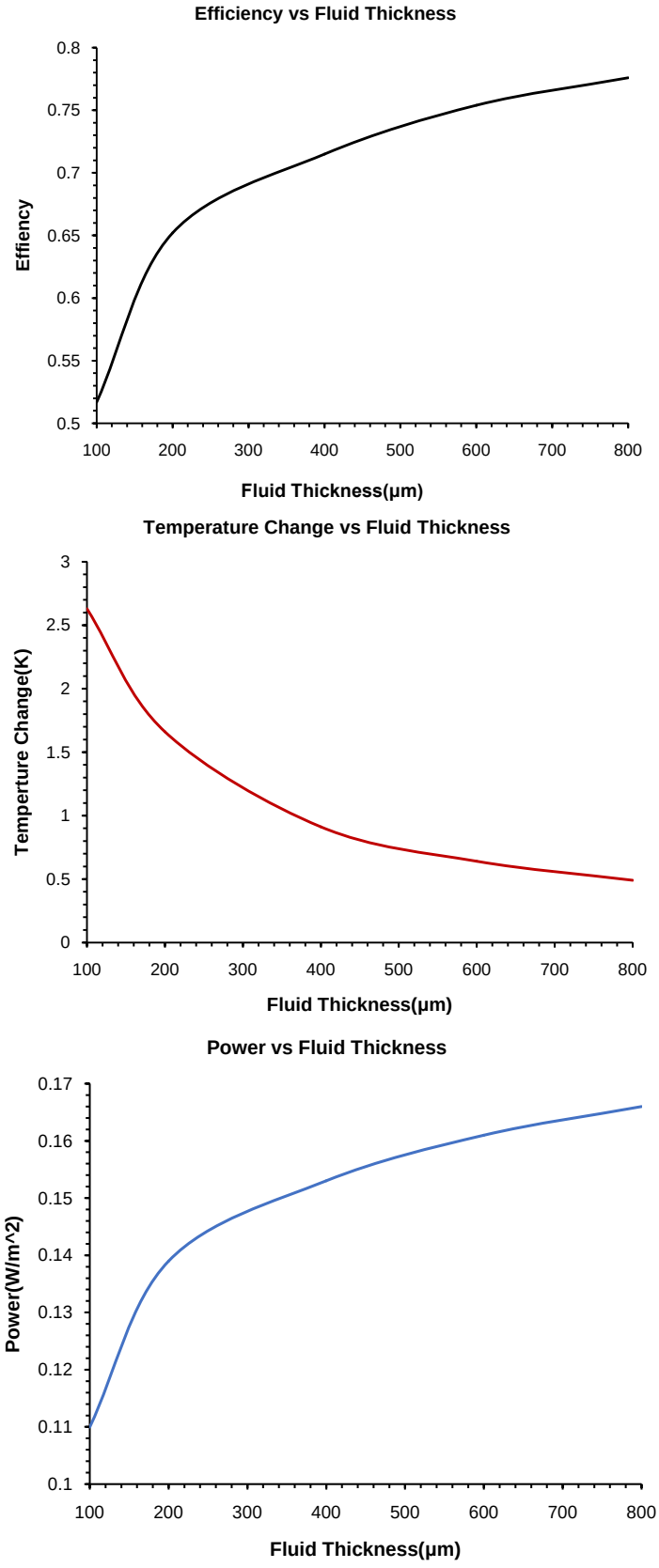


**Figure 4.** Efficiency, temperature change and power change as a function of fluid thickness.

3) Thermal Conductivity of EC Materials

As shown in the Figure 5, while high thermal conductivity of Electrocaloric

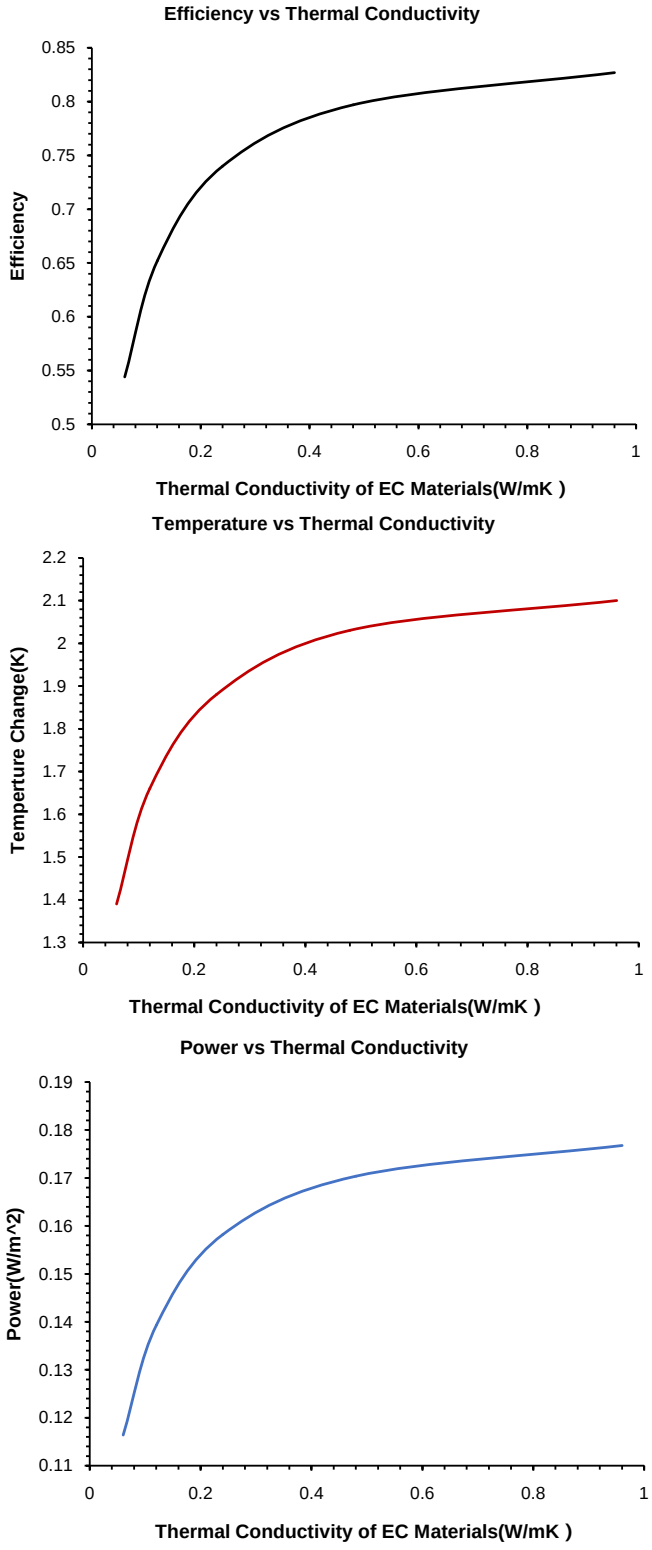


Figure 5. Efficiency, temperature change and power change as a function of thermal conductivity of EC materials.

materials can contribute to EC device performance, the heat generated/absorbed by the ECE requires high thermal conductivity for efficient transport. When the thermal conductivity of EC material increases, efficiency, temperature change of the water, and the power of the model all increases by approximately the same degree. As the thermal conductivity of the EC material increases, more heat can be conducted, which means the heat that transferred from the EC material to the water may be huge, and the process can occur more efficiently. This is made possible by higher temperature change of the liquid-water, the power, and high efficiency of the model. Hence, it can be concluded that it is meaningful to develop EC materials with high thermal conductivity to increase thermal treatment efficiency.

4) The Electric Field Applied

The level of EC temperature change is directly related to both material properties and the voltage applied to the material. Scientists have put significant amounts of efforts to maximize EC temperature change. It has been reported that a temperature change of 50 K has been achieved using a composite material of PVDF based polymer and perovskite nanoparticle. However, high voltage has high requirement for the longevity and stability of EC materials to be used. It is interesting to study the relation between EC device performances (including total device temperature change, power density and energy efficiency) and EC materials temperature change. As we can see from **Figure 6**, when the voltage of the electric field applied increases, the efficiency of the model generally decreases. When the voltage of the electric field applied increases, the increase of the water temperature and the power of the model is approximately linear. The increase of the applied electric field leads to immediate temperature change of the EC material. Thus, the temperature change of liquid water will increase, given that it will absorb more heat. Also, since the water absorbs more energy, the power and efficiency of the use water will also increase. The discrete dots in the first graph indicates that EC temperature change may not be an influential factor of the efficiency. Thus, some minor errors in the simulation may cause some data fluctuation. This partially explains why there isn't a positive correlation in the first graph above.

5) The Thickness of EC Materials

Furthermore, the performance of EC cooling devices is also related to the mass of EC materials used. As shown in the **Figure 7**, When the thickness of EC material increases, the efficiency decreases gradually. When the thickness of EC material increases, dT of water and the power of the model increases at approximately the same level. As the thickness of the EC material increases, more molecules of the material are being utilized. When this happens along with the application of the electric field, more molecules will transform from random movement to orderly movement, which results in an increase in the amount of heat being released. In this way, more heat can be transferred to the water, causing an increase in water temperature and power. However, with the increase of

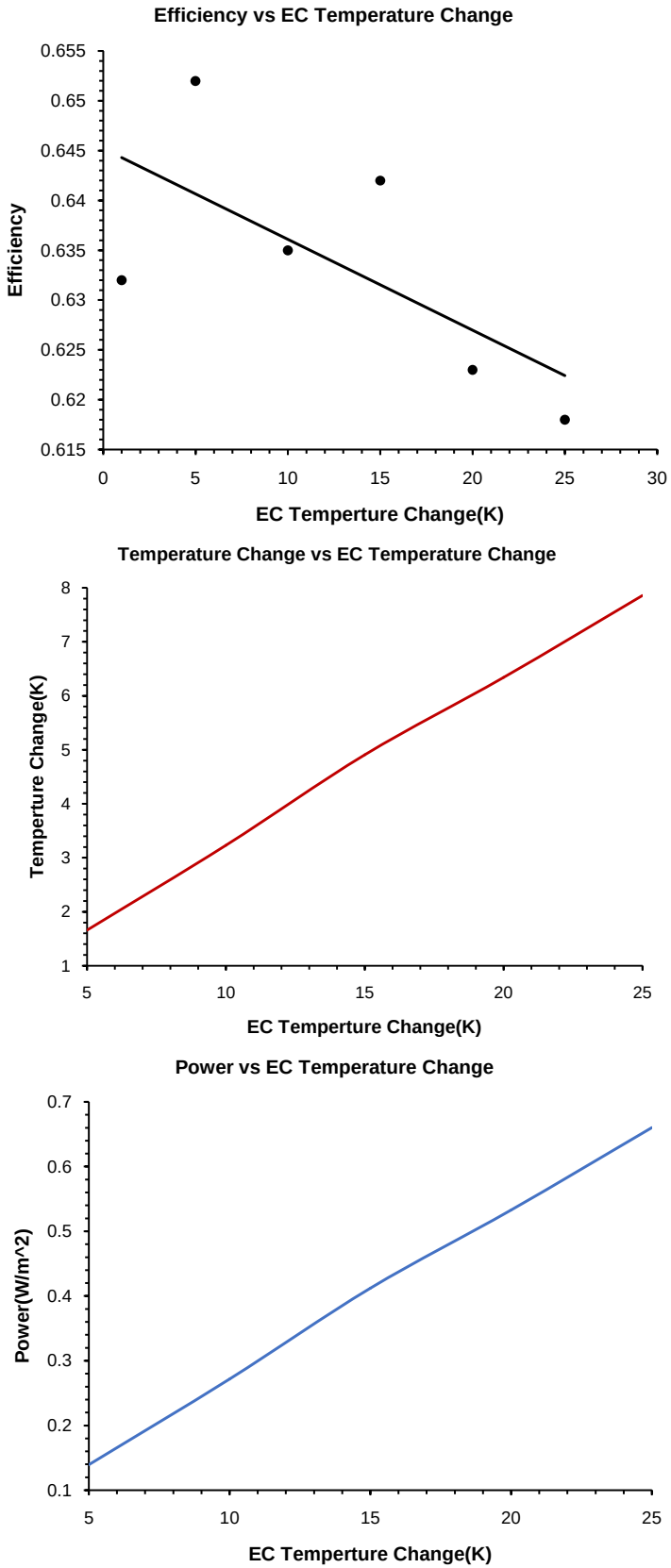


**Figure 6.** Efficiency, temperature change and power change as a function of temperature change of EC materials.

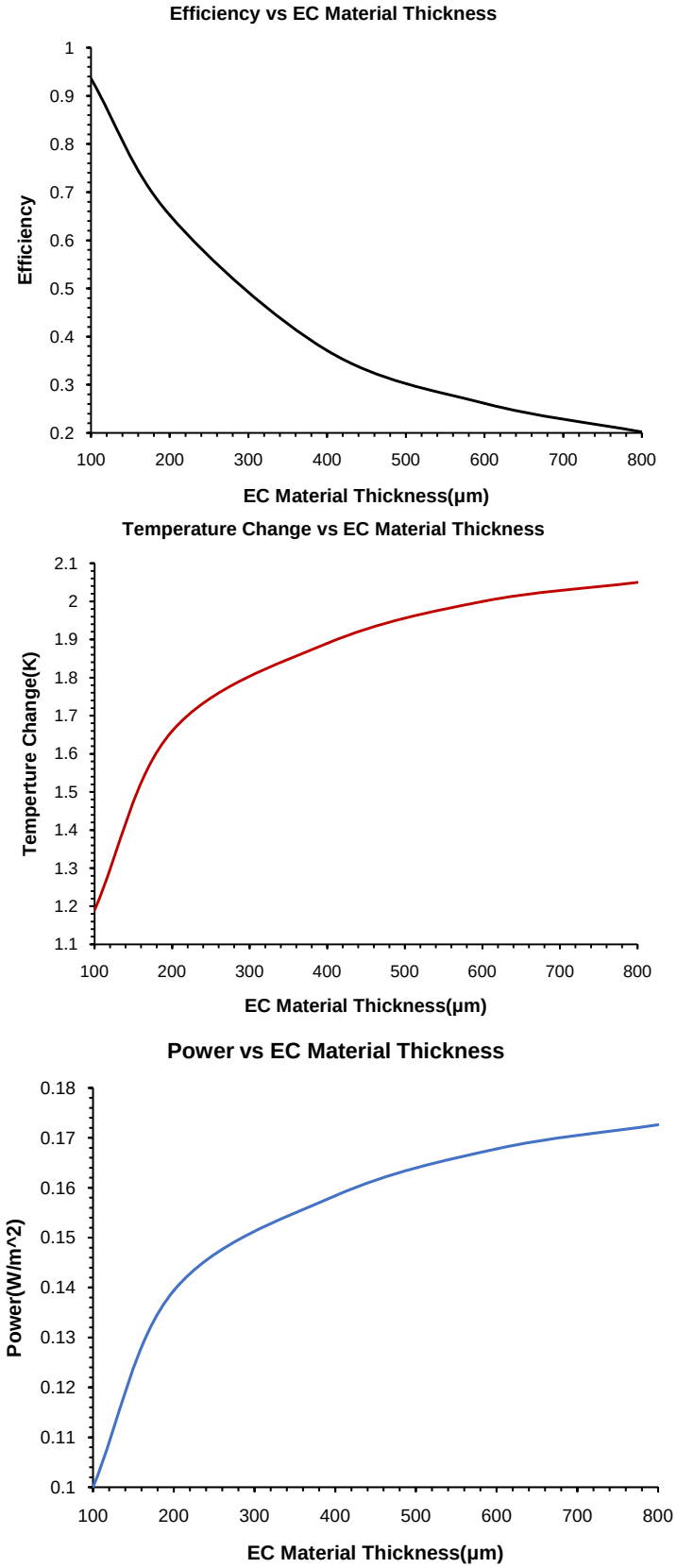


**Figure 7.** Efficiency, temperature change and power change as a function of the thickness of EC materials.

**Table 2.** EC device performance vs cooling fluids.

| liquid | Temperature change (K) | Power (W/cm^2) | efficiency |
|---|---|---|---|
| water | 1.66 | 0.1393 | 0.651610549 |
| glycerol | 1.95 | 0.1178 | 0.551038928 |
| engine oil | 2.48 | 0.085 | 0.397608734 |
| gasoline | 2.44 | 0.079 | 0.369542235 |

EC thickness, the percentage of heat transferred from EC materials to the cooling fluid can be significantly decreased, which lowers the efficiency.

6) The Kind of Liquid Used

As shown from the **Table 2** above, the use of gasoline in the place of cooling fluid can yield the greatest change in temperature, ceteris paribus, while the model that uses water yields the greatest power and best efficiency. The less the value of the specific heat a liquid has, the more temperature change may occur when the same type of electric field is applied.

## 4. Conclusion

In this paper, a compact cooling devices based on Electrocaloric materials has been designed. Factors which affect the performance of the thermal device have also been modeled and analyzed. Finite element simulation shows that a high efficiency can be reached through stated model. It is expected that this study can be a guide for further research in the discovery of better EC materials.

## References

[1] Hirasawa, S., Kawanami, T. and Shirai, K. (2016) Efficient Cooling System Using Electrocaloric Effect. *Journal of Electronics Cooling and Thermal Control*, 78.

[2] Wilson, L. What Are the Major Uses of Electricity? http://shrinkthatfootprint.com/how-do-we-use-electricity

[3] Plaznik, U., *et al.* (2015) Bulk Relaxor Ferroelectric Ceramics as a Working Body for an Electrocaloric Cooling Device. *Applied Physics Letters*, 043903.

[4] CIA World-Fact Book. https://www.cia.gov/library/publications/the-world-factbook/

[5] Joule, J.P. (1859) On Some Thermo-Dynamic Properties of Solids. *Philosophical Transactions*, **149**, 91. https://doi.org/10.1098/rstl.1859.0005

[6] Smith, A. (2013) Who Discovered the Magnetocaloric Effect? *The European Physical Journal*, **38**, 507-517. https://doi.org/10.1140/epjh/e2013-40001-9

[7] Mischenko, A.S., Zhang, Q., Scott, J.F., Whatmore, R.W. and Mathur, N.D. (2006) Giant Electrocaloric Effect in Thin-Film $PbZr_{0.95}Ti_{0.05}O_3$. *Science*, **311**, 1270-1271. https://doi.org/10.1126/science.1123811

[8] Neese, B., Chu, B.J., Lu, S.G., Wang, Y., Furman, E. and Zhang, Q.M. (2008) Large Electrocaloric Effect in Ferroelectric Polymers Near Room Temperature. *Science*, **321**, 821-823. https://doi.org/10.1126/science.1159655

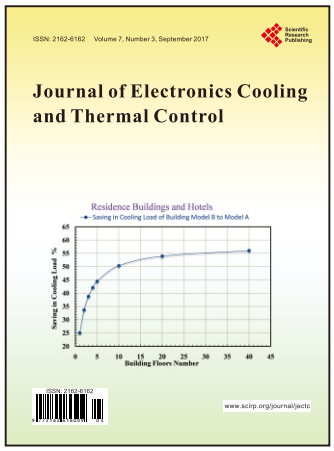


**Call for Papers**

# Journal of Electronics Cooling and Thermal Control

**ISSN 2162-6162 (print) ISSN 2162-6170 (online)**
**http://www.scirp.org/journal/jectc**

**Journal of Electronics Cooling and Thermal Control (JECTC)** is a quarterly, peer-reviewed, academic journal. It aims to provide a vehicle for the exchange and dissemination of original research results, technical notes, and state-of-the-art reviews pertaining to the electronic cooling and thermal system control technology in the computer and electronics industries.

## Subject Coverage

This journal invites original research and review papers that address the following issues. Topics of interest include, but are not limited to:

**Fundamentals and applications of heat/mass transfer processes for the electronics and micro-electronics, such as**

- Base board design and material structure
- Control scenario
- Electronics packaging
- Fan design and performance
- Forced convection heat transfer
- Heat storage
- Heat sink design and optimization
- High heat conductive materials
- Heat transfer in micro channels
- Insulation
- Interface thermal contact performance
- Natural convection heat transfer
- Phase changing heat transfer
- Phonon
- Radiation
- Spray cooling
- Temperature stability
- Thermal modeling of electronics systems and components

**Technologies based on these transport processes such as**

- Enhanced heat/mass transfer in precision-, micro-electronics, information technology
- Heat pipe
- MEMS (Micro-Electro-Mechanical-Systems) and NEMS (Nano-Electro-Mechanical-Systems)
- Various electronic devices, etc.

We are also interested in: 1) Short reports—2-5 page papers where an author can either present an idea with theoretical background but has not yet completed the research needed for a complete paper or preliminary data; 2) Book reviews—Comments and critiques.

## Notes for Intending Authors

The submitted manuscript should not have been previously published in any form and must not be currently under consideration for publication elsewhere. Paper submission will be handled electronically through the website. All papers are refereed through a peer review process. For more details about the submission, please access the website.

## Website and E-Mail

**http://www.scirp.org/journal/jectc** **Email: jectc@scirp.org**

## What is SCIRP?

Scientific Research Publishing (SCIRP) is one of the largest Open Access journal publishers. It is currently publishing more than 200 open access, online, peer-reviewed journals covering a wide range of academic disciplines. SCIRP serves the worldwide academic communities and contributes to the progress and application of science with its publication.

## What is Open Access?

All original research papers published by SCIRP are made freely and permanently accessible online immediately upon publication. To be able to provide open access journals, SCIRP defrays operation costs from authors and subscription charges only for its printed version. Open access publishing allows an immediate, worldwide, barrier-free, open access to the full text of research papers, which is in the best interests of the scientific community.

- High visibility for maximum global exposure with open access publishing model
- Rigorous peer review of research papers
- Prompt faster publication with less cost
- Guaranteed targeted, multidisciplinary audience


Scientific Research Publishing

**Website: http://www.scirp.org**
**Subscription: sub@scirp.org**
**Advertisement: service@scirp.org**